AD-A069 870 CONNECTICUT UNIV STORRS DEPT OF ELECTRICAL ENGINEERI--ETC F/G 5/8
A MODEL FOR THE TARGET TRACKING ABILITY OF A HUMAN OPERATOR IN --ETC(U)
JAN 79 D L KLEINMAN, A R EPHRATH, P K RAO AFOSR-77-3126

UNCLASSIFIED EECS-TR-79-3 NL

1 OF 1
AD
A069870

END
DATE FILMED
7-79
DDC

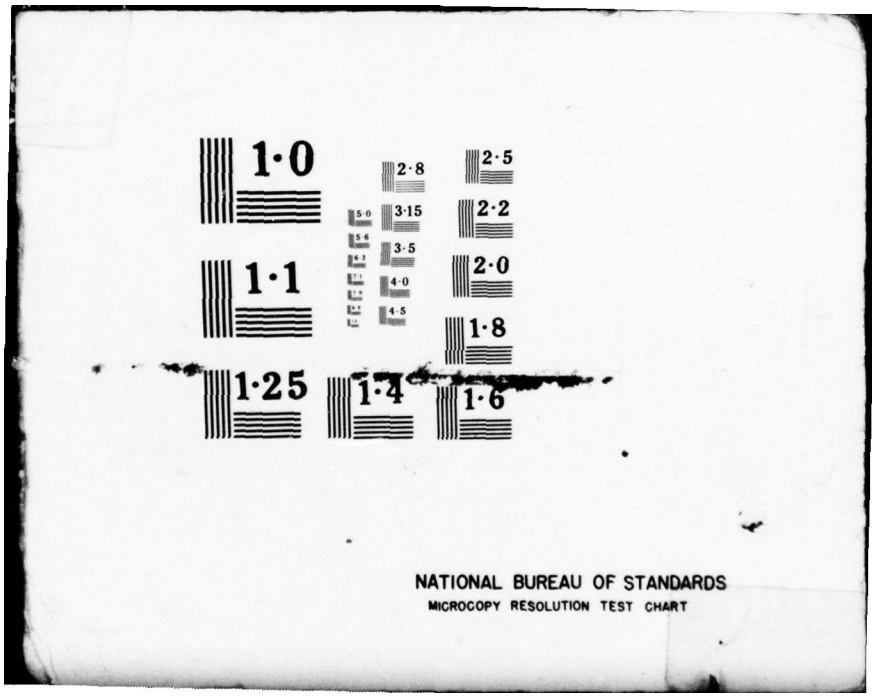
1·0
1·1
1·25
2·8
3·15
3·5
4·0
4·5
5·0
5·6
6·3
1·4
2·5
2·2
2·0
1·8
1·6
NATIONAL BUREAU OF STANDARDS
MICROCOPY RESOLUTION TEST CHART

AFOSR-TR- 79-0677

The University of Connecticut

SCHOOL OF ENGINEERING

Storrs, Connecticut 06268

AD A069870

LEVEL II

DDC FILE COPY

Department of

Electrical Engineering and Computer Science

UNIVERSITY OF CONNECTICUT
DEPARTMENT OF ELECTRICAL ENGINEERING AND COMPUTER SCIENCE

Final Scientific Report. 1 Oct 76 - 30 Nov 78,
for period
Oct. 1, 1976-Nov. 30, 1978

Grant No. AFOSR-77-3126

A MODEL FOR THE TARGET TRACKING ABILITY OF A HUMAN OPERATOR IN AN AAA SYSTEM.

David L. Kleinman,
Arye R. Ephrath
P. Krishna Rao

Technical Report EECS-TR 79-3
January 31, 1979

86 p.
31 Jan 79

Prepared for:

Air Force Office of Scientific Research
Bolling AFB
Washington, D.C. 20332

ABSTRACT

Combined analytic and experimental efforts have expanded our understanding of human information processing and control behavior in target tracking tasks. The research has focused on quantifying the human's "internal" submodel that characterizes his perception of short-term target motion, and on incorporating this construct into the broad-based Optimal Control Model of human response. The final product represents the state-of-the-art with regard to human operator modeling in dynamic Anti-Aircraft Artillery (AAA) systems. Data-vs.-model comparisons of tracking error statistics show that the model can be used with confidence in treating arbitrary target flybys, single-vs.-dual axis tracking loops, visual image cues, and even the effects of temporary visual obscuration. A separate experimental effort studied manned AAA system performance with displayed tracer stream and lead-angle information.

ACKNOWLEDGMENTS

This research project was funded by the Air Force Office of Scientific Research, Life Sciences Directorate, under Grant No. 77-3126 to the University of Connecticut. Contract monitor for the Air Force was Lt. Col. Dominic Maio. Technical monitor for the Air Force was Dr. Carroll Day, AMRL/ME. The support and assistance provided by Air Force personnel was invaluable throughout the project effort. We wish to acknowledge the assistance of Mr. Walt Summers (AMRL/EM) in running the Monte-Carlo simulations, of Mr. Maris Vickmanis (SRL) in the analysis of modeling modifications, and of Mr. George Valentino (AMRL/ME) in providing the impetus for our tracer stream experiments.

At the University of Connecticut, principal investigator was Dr. David L. Kleinman. Dr. Arye R. Ephrath had responsibility for the experimental program and presentation of results. He was given invaluable assistance by Ms. Barbara Chernoff and Mr. Donald Galler. Other graduate student/research assistants were P. Krishna Rao, Roy Lancraft, and Gordon Lee. Report preparation was done by Ms. Catherine Giard and Ms. Paula Kravitz.

TABLE OF CONTENTS

I. INTRODUCTION

The human operator traditionally plays a central role in the target tracking loop of most anti-aircraft artilery (AAA) systems. For example, if the system is engaged in an automatic or autotrack mode, the human's role is primarily that of a monitor and decision-maker. In a manual mode the human is required to accurately track the target using a reticle sight, and fire the weapon. In either case, a complete understanding of the complex inter-relationships between man and machine is essential for quantifying overall weapon system effectiveness or "threat". This understanding, in terms of analytic model representations suitable for computer implementation, is a fundamental goal of the Air Force Manned Threat Quantification (MTQ) program.

Under AFOSR Grant 77-3126, research at the University of Connecticut CYBERLAB has sought to expand our understanding of human information processing and control behavior in manual tracking tasks. Our approach has been to assimilate the results of a joint experimental and analytic program into a precision model for predicting closed-loop man-machine system tracking performance. Applied to manned AAA systems, such a model could be exercised under assumptions of different tracking system/display configurations, different target flyby trajectories, and even different levels of operator proficiency. Clearly, such a model is indispensable to any overall evaluation of manned system effectiveness.

This report details the human operator model that has been developed under this project. Our analytic efforts were well-coordinated with experimental programs both at UConn and at WPAFB, Ohio. Thus, data was used to validate model modifications and, in turn, the models were used to help plan experiments that would further elucidate model structure. The product that has emerged from this cross-fertilization represents the state-of-the art in

modeling human tracking performance in AAA systems. The analytic basis of our work is the well-known Optimal Control Model (OCM) of human response that describes mathematically the salient aspects of human information processing and control behavior. The model is normative in its design, i.e. it attempts to describe what a well-trained, well-motivated operator would do given his control objectives and limitations. Thus, the OCM is well-suited to assimilate new elements of the man-machine system into its framework as they become considered and understood. As a result we have been able to extend the model to treat single-vs.-dual axis tracking, target visual and/or image cues, and even the effects of temporary visual obscuration.

1.1. Background

The suggested use of control-theoretic principles to model human operator response in AAA tracking tasks dates back to the 1946 work of Tustin [1]. However, it has only been of late that the tools of modern control and estimation theory have made the modeling process a reality [2-5]. In two studies conducted during 1972-76, Optimal Control Model predictions were in excellent agreement with manual tracking-error data for the Vulcan (VADS) [3] and S60 [5] weapons system. Moreover, the quality of the model-vs.-data results was uniformly consistent over a variety of (maneuvering) target profiles. The results of these efforts served as the cornerstone for our research project.

Despite the success of the VADS and S60 efforts, it was recognized that numerous assumptions made in the modeling process required further justification and analysis. Moreover, there were facets of human response in target tracking tasks that were not addressed by the earlier studies. It was towards these unanswered questions that AFOSR-supported research at the University of Connecticut, and concomitant efforts at the Aerospace Medical Research Laboratory, WPAFB, have been directed.

The Vulcan study marked the first time that the Optimal Control Model of human response was applied to a significantly non-stationary problem to predict ensemble statistics.† A mechanism was established to treat the non-stochastic nature of the velocity and acceleration profiles associated with a target flyby trajectory. However, the Vulcan study had many shortcomings:

1. Very little data was available with which to validate the model results.
2. Only straight-and-level flyby trajectories were used.
3. Data was available up until target crossover, but not beyond.
4. The target image was of a fixed size, shape and aspect ratio.
5. An ad-hoc scheme was used to model inter-axis (azimuth vs. elevation) attention allocation for the single operator.
6. Questions concerning the human's perception of target motion (i.e.the "internal" model) were left unresolved.

The S60 study, conducted at AMRL, helped to overcome some of the above limitations, but raised others. Fortunately, the Optimal Control modeling technology was transferable in total to the S60 system - - despite the fact that VADS is a disturbed-reticle system while S60 is not, The experimental program produced a wealth of data for model development and validation. Several different a/c trajectories were considered, with data collected well past target crossover. This overcame the limitations (1)-(3) of the VADS study. The shortcoming (4) remained, and, as the S60 system uses separate operators for azimuth and elevation tracking, inter-axis attention allocation (item 5) stayed dormant. However, some limited progress was made towards quantifying the human's internal perception of target motion. For example, it was determined that ensemble mean tracking errors resembled structurally the target's (relative) acceleration profile $\ddot{\theta}(t)$. In addition, a first-order polynomial model was found to be quite adequate for treating perceived target motion. (The VADS study used a second-order model).

---

†Previous applications of the OCM were to steady-state tracking tasks to predict frequency-domain measures.

1.2. Project Overview

The focus of our analytic/experimental modeling efforts is on human information processing and control behavior in target tracking. In order to minimize extraneous complexities such as high-order system dynamics, display/controller nonlinearities, etc., we have considered a simplified k/s tracking loop as shown in Fig. 1. Elevation and Azimuth loops are identical in structure with no dynamic cross-coupling. The use of a basic "stripped-down" tracking loop is not a very restrictive assumption as most tracking systems employ dominant rate-command dynamics, i.e. k/s plus high-frequency filtering. The geometry of the tracking scenario is shown in Fig. 2.

The emphasis of our first year's research was on the effects of target visual cues and dynamic inter-axis attention allocation.

1.2.1 Effects of Target Image and Size.

The experimental program that we conducted used two different trajectories $\theta_T(\cdot)$. A straight-and-level, constant velocity, aircraft flyby was used for baseline work and for comparisons with similar on-going efforts at AMRL. A target fly-by with low-bandwidth random pitching was used to enhance the effects of any visual cues derived from the target image. For each target, two sets of experiments were conducted to study image effects. In one set the target was represented on the CRT display as a triangle of fixed size and shape. In the second set, the target was assumed to be a Δ-shaped aircraft. The image presented on the CRT was the actual contour of the aircraft as would be seen by a human observer. Thus, the image appeared to rotate, change aspect angle and grow in size inversely with range. (In this report the results of only the straight-and-level flyby are presented. See Ref [7] for the complete results of this study).

1.2.2 Effects of Attention Allocation.

Another set of experiments, using only the basic flyby trajectory, were done to isolate the effects of inter-axis attentional allocation. Azimuth and elevation axes were controlled separately, but with elevation and azimuth errors, respectively, held at zero. In this manner full attention was available for single axis control. This set of single-axis tasks was repeated with and without explicit visual cues from the target image.

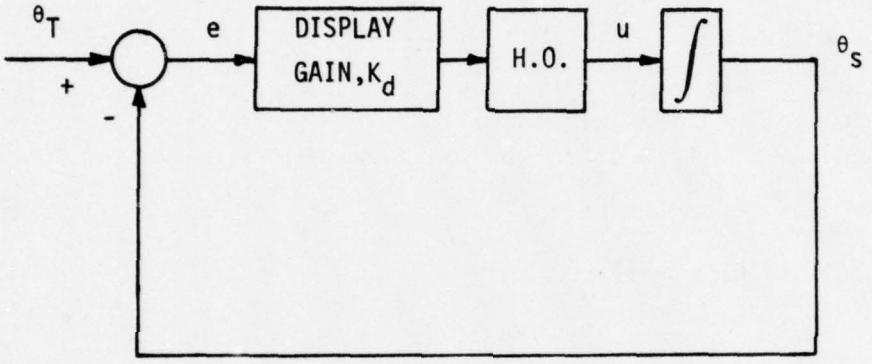

Fig. 1: BASIC TRACKING LOOP

In all experiments the subjects tracked to minimize error, and were scored using an RMS criterion. The human response data collected for each run i=1,...,N were the time histories of tracking error, $e_i(t)$, and control input, $u_i(t)$. For the same experimental condition, these individual time-histories were ensemble-averaged to obtain mean tracking error and standard deviation vs. time. Thus,

$\bar{e}(t)$ = ensemble mean tracking error

$$= \frac{1}{N} \sum_{i=1}^{N} e_i(t) \qquad (1.1)$$

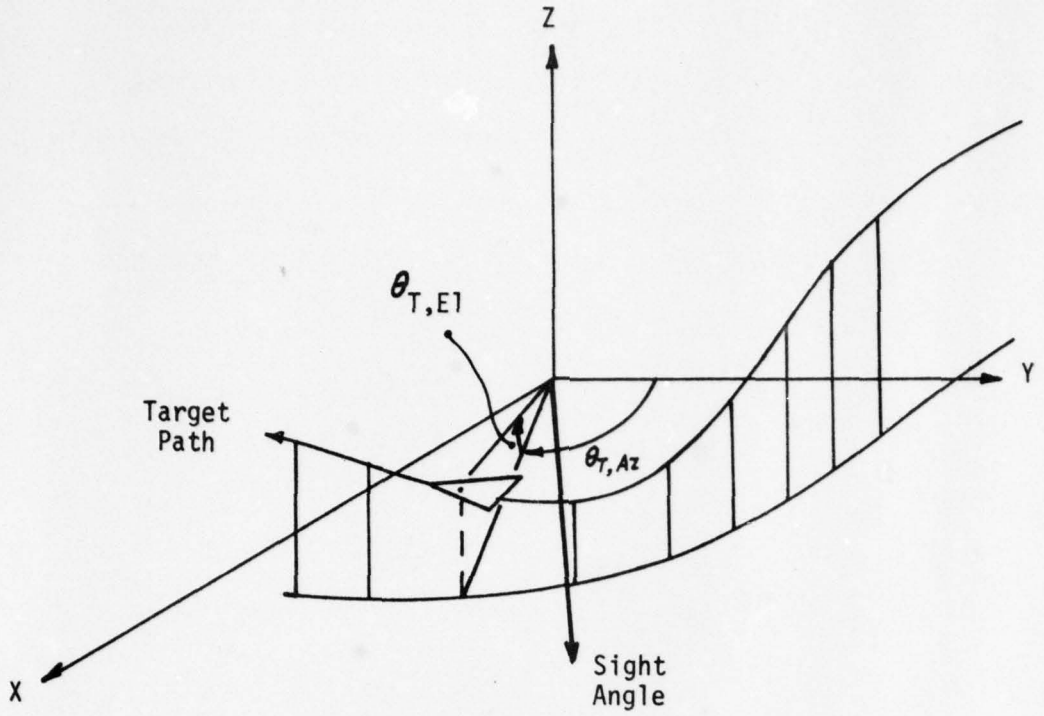

Fig. 2a. Three Dimensional Flight Path and Tracking Geometry

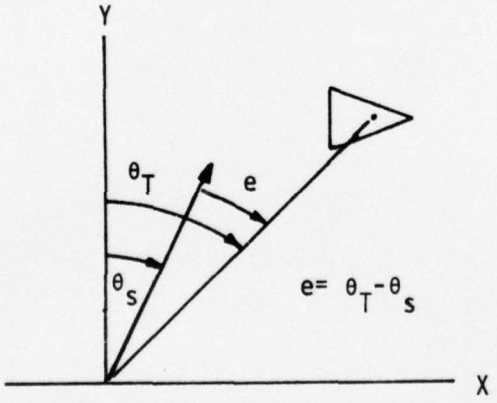

Fig. 2b. Azimuth Axis Plan View

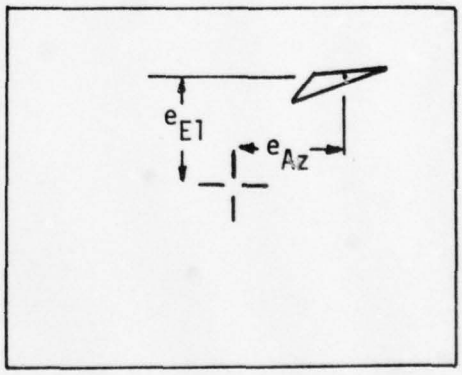

Fig. 2c. Visual Display

$\sigma_e(t)$ = ensemble standard deviation of tracking error

$$= \left\{ \frac{1}{N-1} \sum_{i=1}^{N} [e_i(t) - \bar{e}(t)]^2 \right\}^{\frac{1}{2}} \qquad (1.2)$$

A complete description of our first year's effort, including the experimental procedures and results, may be found in Refs. [6-7].

Our analytic modeling approach aims to reproduce, via computer simulation, the ensemble statistics $\bar{e}(t)$ and $\sigma_e(t)$ for each configuration/target profile considered. The Optimal Control Model of human response, modified to treat the non-stationary aspects of the tracking task, served as the analytic basis for our work [8]. Additional modifications to the OCM were made during the first year: Target visual cues were modeled as a direct perception of target velocity, $\dot{\theta}_T$. Inter-axis attention was assumed to be allocated by the human to optimize his information base. Motivated by the results of Refs. [3] and [9], a dynamic attention allocation scheme was proposed and evaluated vis-à-vis the data. Results are given in Ref. [7] and summarized in Section 2.1. Qualitatively, visual cues improve performance while attention sharing degrades performance, as expected. Our modeling work quantifies these effects and others.

A major conclusion of the first year's effort was that in order to reproduce certain asymmetric and structural trends in the human response data, an adaptive (first-order) model representation of target angular velocity, $\dot{\theta}_T$, was needed. Accordingly, a major part of the second year's effort focused on describing the human's "internal" model that characterizes his perception of short-term target motion. Concomitant adaptive schemes that use this model to generate estimates of target velocity and acceleration, as proposed in [7], were refined. The complete tracking model developed under this project is presented in Chapter II, along with data-model comparisons.

Our method to infer the "internal" model used a set of tracking experiments designed to accentuate the role of this model in the operator's response. Via experiment we studied manual tracking performance as modified by short periods (1 sec) of target blanking. During the blanking period, the human operator's performance is governed almost entirely by his internal model construct of the target motion, as there is no visual information. The ensemble data from these blanking experiments were used to suitably refine/validate the overall man-machine tracking model, including the target submodel.

Although the blanking data was integral to the model-building process of Chapter II, we present the blanking results separately. Thus, Chapter III is devoted solely to the blanking study. The data-vs.-model results validate--via acid test--the form of the internal model, and its use within a hierarchial Optimal Control tracking model. These results are significant from a purely theoretical viewpoint. From an applications viewpoint, the tracking model can be used to study temporary obsuration of a target due to optical/electronic countermeasures, terrain, etc., and the resultant effect on system performance.

Having reached a logical "plateau" in model development, our interest turned to methods for improving overall AAA system effectiveness[+] by means of display/dynamic element modifications. Motivated by MTQ project work at AMRL, we studied the use of tracer information in target tracking. (Most AAA weapons systems utilize information from tracer rounds). If the tracking system contains a synthetic CRT display, it is then relatively easy to present computer-generated tracer information to the human. Only the format of this presentation is at issue. Our experimental program considered tracking with the display showing i) a full tracer stream ending at the target's present range, or ii) only the endpoint of the tracer stream at the target's range. The experimental results, which demonstrate convincingly the superiority of (i), are found in Chapter IV.

[+] as measured by "hit score" as opposed to tracking error

There were several other topics studied during the project effort that are not described in this report, but are documented elsewhere. These include the following.

1.2.1. Monte-Carlo Simulation of Human Operator Response [7, 10].

The OCM is used typically to predict ensemble, or averaged statistics of system response. A major effort during the first year of the grant was the implementation of the OCM equations for Monte-Carlo, or sample path, simulations. The simulation generates time-histories of tracking error, control input, etc., in response to any given target trajectory. Thus, the model mimics the input-output response of the human operator, complete with random noise generators that reproduce inherent human randomness. Using a Monte-Carlo model one can study performance measures not readily available from the averaged ensemble statistics such as:

1. Oscillation frequencies in the responses, including spectral content over time windows.
2. Autocorrelation and cross-correlation functions.
3. Effects of transient phenomena and other time-domain oriented items.

Theoretically, the ensemble statistics of model-generated waveforms must agree with the OCM covariance propagation results obtained directly. Moreover, it is interesting to examine (numerically) the smoothing inherent in the ensemble averaging process, of Eq. (1.1), using computer-generated data, to see the characteristics of $\bar{e}(t)$ vs. N as $N \to \infty$. This was done for the S60 system for N=1, 16, and 100. These results were then constrasted with actual ensemble-averaged data and with covariance propagation model results.

1.2.2. A Study of Motor Structures in the Optimal Control Model [11,12]

Recent interests in modeling the effects of motion on human performance, and in manual control of low-bandwidth systems has lead to the need for accurate submodels of the"neuro-motor" characteristics of the human operator.

Unfortunately, matching low-frequency human response data has been a problem with almost all operator models, the OCM being no exception. This study was an attempt to better understand, to put in perspective, and hopefully eliminate these problems.

In this study, the properties of several structural variations in the neuromotor interface portion of the OCM were investigated. One technique suggested in [13-14] introduces a pole at s=0 in the feedback loop which, in turn, generates low-frequency phase and magnitude characteristics similar to experimental data. However, this gives rise to unusually high sensitivities with respect to model noise parameters, thereby degrading the model's predictive capabilities. These sensitivities were analyzed, and modifications to the model were investigated, including the effects of explicit proprioceptive cues obtained via the neuro-motor pathways. The analysis dealt mostly with k/s system dynamics so that the results would have direct application to the AAA tracking loop, and ultimately to the design of manipulator characteristics.

1.2.3. Identification of Parameters in the Optimal Control Model [15-16]

The main objective of our model-data comparisons was to determine a suitable tracking model structure, i.e. internal target submodel, adaptive estimation scheme, etc. This was accomplished using a nominal set of OCM parameters that relate to the operator's inherent limitations. Once the structure is determined, the next step is to fine-tune the model-data match via a parameter identification scheme. This latter process has typically been done using trial-and-error methods, i.e. by "eye-ball".

Our research was directed towards developing an automated scheme for identifying OCM parameters from human response data. Due to the complexity of the problem, our initial efforts dealt with steady-state models using transfer-function, remnant and scores data. During 1977-78 we were fortunate to have the services of Prof. Björn Wittenmark, an expert in identification,

who was on leave from Lund Institute of Technology, Sweden. Together with inputs from personnel at Bolt Beranek and Newman, Inc., a loss function was formulated to reflect model-vs.-data differences. The loss function weights model-vs.-data differences inversely proportional to measured uncertainties. Several non-linear programming techniques were developed to minimize the loss function by adjusting model parameters. The techniques worked well for the steady-state models. Their extension to non-stationary model parameter identification, using ensemble data (necessary for AAA system), is an item of on-going research.

II. ANALYTIC MODEL FOR MANUAL TRACKING

This chapter describes the various modifications and extensions that were made to the Optimal Control Model (OCM) to treat the deterministic structure of a target flyby. These include adaptive tracking of target acceleration, internal model characterization of target velocity, and methods for modeling visual cues and attentional allocation. Model predictions of first-and second-order error statistics are compared with experimental results.

2.1 Model Formulation

The closed-loop structure of the compensatory tracking task was shown in Fig. 1. The human controls a rate-command sight, $\dot{\theta}_s(t)=u(t)$, so as to minimize the observed tracking error $e(t)=\theta_T(t)-\theta_s(t)$. Defining states $\underline{x}_0' = [x_1,x_2] = [\dot{\theta}_T, e]$ the system dynamics for either elevation or azimuth axis of control is given by

$$\dot{x}_1(t) = z(t) \quad ; \; z(t) = \ddot{\theta}_T(t) \tag{2.1a}$$

$$\dot{x}_2(t) = x_1(t) - u(t) \tag{2.1b}$$

The displayed information consists of tracking error e(t), error rate $\dot{e}(t)$ and target velocity $\dot{\theta}_T$ in those cases where there are realistic target image cues [7]. Thus,

$$\underline{y}(t) = C_0\underline{x}_0(t) + D_0u(t) = \begin{bmatrix} 0 & 1 \\ 1 & 0 \\ 1 & 0 \end{bmatrix} \underline{x}_0 + \begin{bmatrix} 0 \\ -1 \\ 0 \end{bmatrix} u \tag{2.2}$$

for azimuth and/or elevation axes. The human is assumed to perceive a signal that is delayed noisy replica of $\underline{y}(t)$,

$$\underline{y}_p(t) = \underline{y}(t-\tau) + \underline{v}_y(t-\tau) \; ; \quad \tau = .2 \text{ sec} \tag{2.3}$$

where $\underline{v}_y(t)$ are independent white-noises with a covariance matrix $V_y(t)$ that depends

on the statistics of $\underline{y}(t)$.

The application of the Optimal Control Model of human response to obtain performance predictions requires a state-space representation of the system dynamics in order to compute optimal control and filter gains. Generally, this "internal" model is identical to the system model Eq. (2.1). However, in cases where the dynamics being controlled are of high-order, or where external inputs have a complex structure, non-isomorphic models may be more realistic [21]. The latter situation is appropriate to the present case. Here it is necessary for us to write a state-space (Markov) model for the target motion $x_1 = \dot{\theta}_T$ to include in the OCM.

On the basis of first-vs-second order model analysis as reported in [6-7], we assume a generalized "internal" model for the target velocity,

$$\dot{x}_1(t) = -\alpha(t)x_1(t) + w_d(t) \tag{2.4}$$

where $w_d(t)$ is assumed to be a white-gaussian noise with covariance $W_d(t)$. In the "truth model"

$$\dot{x}_1(t) = -\alpha(t)\, x_1(t) + z(t) \; ; \; z(t) = \ddot{\theta}_T + \alpha\dot{\theta}_T \tag{2.5}$$

which is equivalent to Eq. (2.1a). The implication of Eq. (2.4) versus Eq. (2.5) is that the human operator has no explicit information regarding $z(t)$, and must model its effect as that of a white-noise with suitable covariance $W_d(t)$. The usual choice for $W_d(t)$ is [3,8],

$$W_d(t) = 2\tau_c\, z^2(t) \tag{2.6}$$

where τ_c is the "correlation time" of the $z(\cdot)$ process. Of course, $z(t)$ is unknown to the human so that an estimate, $\hat{z}(t)$, will ultimately be required in Eq. (2.6). The parameter $\alpha \geq 0$ represents the "local" bandwidth of the signal x_1 at time t. Note that Eq. (2.4) is, hypothetically, a rate-smoothing mechanism. The actual system dynamics are thus represented by

$$\dot{\underline{x}}_0 = \begin{bmatrix} -\alpha & 0 \\ 1 & 0 \end{bmatrix} \underline{x}_0 + \begin{bmatrix} 0 \\ -1 \end{bmatrix} u + \begin{bmatrix} 1 \\ 0 \end{bmatrix} z(t) \tag{2.7}$$

which is in the requisite form for Optimal Control Model analysis,

$$\dot{\underline{x}}_0(t) = A_0 \underline{x}_0(t) + B_0\, u(t) + F_0\, z(t) \tag{2.8}$$

In the OCM the human's feedback control strategy is modeled by

$$\dot{u}(t) = -[L_1, L_2, L_3] \begin{bmatrix} \hat{\underline{x}}_0 \\ u \end{bmatrix} + v_u(t) = \dot{u}_c(t) + v_u(t) \tag{2.9}$$

or, equivalently

$$\tau_n\, \dot{u}(t) + u(t) = \tau_n [L_1, L_2]\, \hat{\underline{x}}_0 + \tau_n v_u(t) \tag{2.9a}$$

where $\tau_n = L_3^{-1}$. The control gains $L = [L_1, L_2, L_3]$ are selected to minimize a combination of mean-squared tracking error plus control rate,

$$J(u) = \lim_{T \to \infty} \frac{1}{T}\, E \int_0^T [y_1^2(t) + g\, \dot{u}^2(t)]\, dt \tag{2.10}$$

Since α is not necessarily constant the gains L_i would in theory, be functions of time. To simplify the modeling process, consistent with limitations on human knowledge of future α, we use the steady-state gains associated with the present α. Solving the 3 x 3 Riccati equation associated with the optimal control problem gives (with $g = .0004$ corresponding to $\tau_n = .1$),

$$L_3 = \tau_n^{-1} = 10 \; ; \; L_2 = -50 \; ; \; L_1 \simeq -10 + \alpha \tag{2.11}$$

Note that the gains L_2 and L_3 are not α-dependent. The motor noise $v_u(t)$ in Eq. (2.9) is white, gaussian with covariance $V_u(t)$ that scales with commanded control rate, $\dot{u}_c(t)$, viz,†

---

†We have found that this scaling provides a better model for motor randomness than does scaling with control u(t).

$$V_u(t) = \pi\rho_u \, E\{\dot{u}_c^2(t)\} \; ; \; \rho_u \simeq .01 \tag{2.12}$$

The state estimate $\underline{\hat{x}}(t) = [\underline{\hat{x}}_0, \hat{u}]'$ is generated by an (augmented) Kalman filter and linear predictor that compensate, in turn, for the human's inherent randomness and time-delay. Defining

$$\underline{p}(t) = E\{\underline{x}(t-\tau) \,|\, \underline{y}(\sigma), \; \sigma \leq t\} \tag{2.13}$$

the filter equation is

$$\dot{\underline{p}}(t) = A\underline{p}(t) + B\mu(t-\tau) + G(t)\,[\underline{y}_p(t) - C\underline{p}(t)] \tag{2.14}$$

where $\mu(t) = -[L_1, L_2]\,\underline{\hat{x}}_0(t)$ and

$$A = \begin{bmatrix} A_0 & B_0 \\ 0 & -L_3 \end{bmatrix} \; ; \quad B = \begin{bmatrix} \underline{0} \\ 1 \end{bmatrix} \; ; \; C = [C_0, D_0]$$

The state prediction is obtained by integrating the equation

$$\frac{d}{dt}\,\underline{\hat{x}}(\sigma) = A\,\underline{\hat{x}}(\sigma) + B\mu(\sigma) \qquad t-\tau < \sigma \leq t \tag{2.15}$$

from $\sigma = t-\tau$ to $\sigma = t$ with initial condition $\underline{\hat{x}}(t-\tau) = \underline{p}(t)$

The filter gain $G(t) = \Sigma(t)C'V_y^{-1}(t-\tau)$ where $\Sigma(t)$ is generated from the Riccati equation

$$\dot{\Sigma} = A\Sigma + \Sigma A' - \Sigma C' V_y^{-1}(t-\tau) C\Sigma + \mathrm{diag}[F_0 W_d F_0', V_u] \tag{2.16}$$

with W_d and V_u given by Eqs. (2.6) and (2.12), respectively. The filtering error $\underline{e}_f(t) = \underline{x}(t-\tau) - p(t)$ satisfies the differential equation

$$\begin{aligned} \dot{\underline{e}}_f(t) &= A\,\underline{e}_f(t) - G(t)\,[\underline{y}_p(t) - C\,\underline{p}(t)] + B\,v_u(t-\tau) + F\,z(t-\tau) \\ &= (A-GC)\,\underline{e}_f(t) - G(t)\,\underline{v}_y(t-\tau) + B\,v_u(t-\tau) + F\,z(t-\tau) \end{aligned} \tag{2.17}$$

where $F = [F_0, 0]'$. Because of the "suboptimal" nature of the Kalman filter, wherein $z(t)$ is replaced by a white-noise, we note that $\Sigma(t) \neq \mathrm{cov}\,[\underline{e}_f(t)] = E_f(t)$. This latter quantity is given by

$$\dot{E}_f(t) = (A-GC)\, E_f(t) + E_f(t)\, [A-GC]' + G\, V_y(t-\tau)\, G' + B\, V_u(t-\tau)\, B' \quad (2.18)$$

The mean of the filtering error $\bar{e}_f(t)$ is given by

$$\dot{\bar{e}}_f(t) = (A-GC)\, \bar{e}_f(t) + F\, z(t-\tau) \quad (2.19)$$

The elements of the diagonal observation noise covariance $V_y(t)$ are

$$V_{yi}(t) = \frac{\pi \rho_{yi}}{f_i N_i^2}\, E\{y_i^2(t)\} \quad ; \rho_{yi} \sim .01 \quad (2.20)$$

There is assumed to be no intra-axis attention allocation among the 3 observations, $\underline{y} = \{e, \dot{e}, \dot{\theta}_T\}$. Thus $f_i = f_A$ or f_E is the attention to either the azimuth or elevation axis tracking task, as the case may be. The method we have recommended for computing f_A/f_E as a function of time is [7]:

$$f_A = (1+R^2)^{-1} \quad ; R = \frac{(L_e \Sigma L_e')_E}{(L_e \Sigma L_e')_A} \quad (2.21)$$

$$f_E = 1 - f_A$$

where $L_e = \sqrt{g}\, L\, e^{A\tau}$ is an "equivalent" gain. Finally, the quantity N_i is the RIDF (random input describing function) gain of a visual/indifference threshold of width $\pm a_i$.

2.2 Selection of Internal Model Parameters

OCM predictions of tracking error ensemble statistics, generated using nominal values for the parameter set

$$\Omega = \{\tau,\ \rho_u,\ \tau_n,\ a_i,\ \rho_{yi}\}$$

and selecting

$$\tau_c = .5 \text{ sec} \quad (2.22a)$$

$$\alpha(t) = 3\sqrt{\Sigma_{11}(t)}\ /57.3 \quad (2.22b)$$

gave mixed results when compared with data [7]. Azimuth model vs. data comparisons were adequate, but elevation axis results did not agree well. Moreover, this model

was found to be lacking considerably when applied to predict the results of the blanking experiments (see Chapter III). It is possible to trace the roots of the mismatches to the internal model characterization of the target dynamics -- i.e. to the selection of τ_c and $\alpha(t)$.

The form of Eq. (2.22b) for $\alpha(t)$ was suggested by an uncertainty minimization arguement applied to tr $\dot{\Sigma}(t)$. The constant value $\tau_c \sim .5$ sec was associated with human short-term memory, and not with the target motion per se. In retrospect, this was not a good choice, inasmuch as τ_c represents a correlation time for the $z(t)$ process. The correlation time for the $x_1 \simeq \dot{\theta}_T$ process, using the model (2.4), is $1/\alpha$. Since $z(t)$ is primarily the derivative of x_1, a smaller -- but nevertheless related -- correlation time for $z(t)$ could be expected. We assume that the "bandwidth" of the differentiated signal is twice that of the original signal. Thus,

$$\tau_c = 1/2\,\alpha \tag{2.23}$$

so that τ_c becomes a function of time, linked with $\alpha(t)$.

The selection of $\alpha(t)$ remains to be determined. A heuristic approach for obtaining a <u>structural</u> form for $\alpha(t)$ imposes a quasi-stationary mean-square equivalence between the outputs of Eqs. (2.4) and (2.5). At time t we project $E\{x_1^2(t)\}$ to its steady-state value keeping $\alpha(t)$ and $W_d(t)$ fixed. Letting $\bar{X}$ denote this number, we have with Eq. (2.23),

$$0 = -2\alpha(t)\,\bar{X} + \frac{1}{\alpha(t)}\,z^2(t)$$

Since $x_1(t)$ is supposed to represent $\dot{\theta}_T(t)$ to some extent, we impose the equivalence

$$\bar{X} = \dot{\theta}_T^{\,2}(t)$$

which requires

$$\alpha(t) = \beta\sqrt{\frac{z^2(t)}{\dot{\theta}_T^{\,2}(t)}} \quad ; \quad \beta = .707 \tag{2.24}$$

Equation 2.24 gives only a structural form for $\alpha(t)$ owing to the nature of the approximation inherent in its development. It is an <u>implicit</u> equation for $\alpha(t)$ in terms of quantities $z(t)$ and $x_1(t) = \dot{\theta}_T(t)$ that appear in the internal model formulation. Since $z(t)$ is itself a function of $\alpha(t)$, it is of interest to derive an <u>explicit</u> equation for $\alpha(t)$. Substituting $z = \ddot{\theta} + \alpha\dot{\theta}$ into Eq. (2.24) and solving for the positive root gives,

$$\alpha(t) = \frac{\beta}{1-\beta \operatorname{sgn} \frac{\ddot{\theta}}{\dot{\theta}}} \cdot \frac{|\ddot{\theta}(t)|}{|\dot{\theta}(t)|} = C_\theta \frac{|\ddot{\theta}|}{|\dot{\theta}|} \tag{2.25}$$

Thus, $\alpha(t)$ is proportional to the ratio $\ddot{\theta}/\dot{\theta}$, which is often used as a measure of local bandwidth. Note however, that the proportionality factor depends on whether the target speed is increasing or decreasing! If $\ddot{\theta}$ has the same sign as $\dot{\theta}$ a larger estimate (bandwidth) for $\alpha(t)$ will be generated, vs the case where $\ddot{\theta}$ and $\dot{\theta}$ have opposite signs. This has some intuitive appeal in terms of a "doppler" shift characteristic.

The original development of Eq. (2.22) presupposed that $\alpha(t)$ was chosen to minimize $\dot{\Sigma}_{11}(t)$. It is of interest to repeat this approach, using the assumption (2.23). Letting $\tau=0$ for simplicity:

$$\dot{\Sigma}_{11} = -2\alpha\, \Sigma_{11} + \frac{1}{\alpha}(\ddot{\theta} + \dot{\theta})^2 + \text{terms indep of } \alpha.$$

Setting $\partial\Sigma_{11}/\partial\alpha = 0$ gives

$$\alpha(t) = \sqrt{\frac{\ddot{\theta}^2(t)}{\dot{\theta}^2(t) - 2\Sigma_{11}(t)}} \tag{2.26}$$

Due to the scaling nature of the noise processes in the OCM, one might expect $\Sigma_{11}(t) = \varepsilon\, \dot{\theta}^2(t)$ where $\varepsilon > 0$ is larger when $\ddot{\theta}$ and $\dot{\theta}$ have the same sign ($z(t)$ is bigger in this case). Thus, Eq. (2.26) gives, albeit heuristically, the same

structural form for $\alpha(t)$ as does Eq.(2.24) or (2.25).

2.3 Internal Model Implementation

In order to implement Eq. (2.24) for $\alpha(t-\tau)$ in the OCM it is necessary to replace the quantities $\dot{\theta}_T^2(t-\tau)$ and $z^2(t-\tau)$ with obtainable estimates. Note that an estimate of $z(t-\tau)$ is also needed to form $W_d(t-\tau)$. An estimate of $\dot{\theta}_T^2(t-\tau)$ is readily available from the Kalman filter ensemble[+] statistics,

$$\dot{\theta}_T^2(t-\tau) = \bar{p}_1^2(t) + \Sigma_{11}(t) \tag{2.27}$$

where $\bar{p}_1(t)$ is the ensemble mean of the estimate $p_1(t)$. Note that Σ_{11} has been used as the (human's) approximation to $\mathrm{cov}[\underline{e}_f(t)]$.

A method for estimating $z(t-\tau)$ is not as straightforward. A least-squares approach, using the Kalman filter innovations sequence, was proposed and implemented in Ref. [7]. The main idea is that since it is the signal $z(t)$ that gives rise to the ensemble mean statistics via the mean filtering error equation, Eq. (2.19), we have

$$\dot{\bar{\underline{e}}}_f(t) = A(t-\tau)\,\bar{\underline{e}}_f(t) - G(t)\,\bar{\underline{\nu}}(t) + F\,z(t-\tau) \tag{2.28}$$

where $\bar{\underline{\nu}}(t)$ is the mean innovations in the Kalman filter,

$$\bar{\underline{\nu}}(t) = C\,\bar{\underline{e}}_f(t) = E\{\underline{y}_p(t) - C\,\underline{p}(t)\} \tag{2.29}$$

By "measuring" $\bar{\underline{\nu}}(t)$ -- the signal $\underline{\nu}(t)$ being readily available in the Kalman filter -- we can obtain an estimate of $z(t-\tau)$, essentially by designing the inverse system to Eqs. (2.28-2.29).

Solving Eqs. (2.28-2.29) for $\bar{\underline{\nu}}$, assuming $\bar{\underline{e}}_f(0) = \underline{0}$, gives

---

[+]Ensemble statistics are used to obtain "averaged" behavior, inasmuch as model predictions are generated via covariance propagation formulae.

$$\underline{\bar{\nu}}(t) = C\int_0^{t-\tau} \Phi(t-\tau,\sigma)\ [F\ z(\sigma) - G\ \underline{\bar{\nu}}(\tau+\sigma)]d\sigma \qquad (2.30)$$

where Φ is the state transition matrix associated with $A(t-\tau)$. If $\hat{z}(\sigma|t)$, $\sigma<t-\tau$ denotes the estimate of $z(\sigma)$ given all the measurements $\underline{\bar{\nu}}(\sigma)$, $\sigma<t$, then our best estimate of $\underline{\bar{\nu}}(t)$ is

$$\underline{\bar{\nu}}(t) = C\int_0^{t-\tau} \Phi(t-\tau,\sigma)\ [F\ \hat{z}(\sigma|t) - G\ \underline{\bar{\nu}}(\tau+\sigma)]\ d\sigma \qquad (2.31)$$

The estimates $\hat{z}(\sigma|t)$ can be obtained via a (weighted) least-squares method to minimize the criterion

$$J_\nu = \int_0^t e^{-2\gamma(t-\xi)}\ \left\|\underline{\bar{\nu}}(\xi) - \underline{\hat{\bar{\nu}}}(\xi)\right\|^2_{R^{-1}(\xi)}\ d\xi \qquad (2.32)$$

where $R(\xi)$ is a diagonal matrix that weights the relative importance of each measurement $\bar{\nu}_j$, $j=1,\ldots,NY$. Plausible choices are $R=V_y$ or $R=I$. The constant $\gamma>0$ is a fading memory factor used to place greater emphasis on the more recent data, consistent with human processing.

The minimization of J_ν is a formidable process as it requires the recomputation (i.e., smoothing) of past estimates using all the past data $\underline{\bar{\nu}}(\sigma)$, $\sigma<t$. In order to develop a scheme that is more amenable to human operator modeling, we simplify the WLS problem by replacing the <u>smoothed</u> estimate in Eq. (2.31) with the <u>filtered</u> estimate $\hat{z}(\sigma|\sigma) = \hat{z}(\sigma)$. The minimization of J with respect to this quantity follows recursive least-squares theory. Define the "effective" measurement as

$$\underline{\tilde{y}}(t) = \underline{\dot{\bar{\nu}}}(t) - CA\ \underline{\hat{\bar{e}}}_f(t) + CG(t)\ \underline{\bar{\nu}}(t) \qquad (2.33)$$

where

$$\underline{\hat{\bar{e}}}_f(t) = \int_0^{t-\tau} \Phi(t-\tau,\sigma)\ [F\ \hat{z}(\sigma) - G\ \underline{\bar{\nu}}(\tau+\sigma)]\ d\sigma$$

Then, $\tilde{\underline{y}}(t) = CFz(t-\tau) + \text{"noise"}$, where the residual "noise" is $CA(t-\tau)\cdot[\bar{\underline{e}}_f(t) - \hat{\underline{e}}_f(t)]$ and $z(t-\tau)$ may be generated recursively, in continuous time, by

$$\dot{\hat{z}}(t-\tau) = P(t)\ F'C'\ R^{-1}(t-\tau)\ [\tilde{\underline{y}}(t)-CF\ \hat{z}(t-\tau)] \tag{2.34}$$

$$\dot{P}(t) = 2\gamma P(t) - P(t)\ F'C'R^{-1}(t-\tau)\ CF\ P(t) \tag{2.35}$$

The actual implementation of the WLS algorithm is done in a discrete-time form as described in [7]. This avoids some of the subtleties involved in the differentiation of $\bar{\underline{v}}(t)$, and is compatible with the discrete-time propagation of the ensemble mean and covariance equations. This algorithm for estimating $z(t-\tau)$ requires minimal computation (since F is a vector), and minimal storage requirements. With $\gamma \sim 1/.25\ \text{sec}^{-1}$ the technique has been remarkably successful in generating an estimate $\hat{z}(t-\tau)$ that accurately "tracks" $z(t-\tau)$ for all target profiles considered to date. In summary, then, the internal model parameters for use in the OCM are

$$\alpha(t-\tau) = \beta \sqrt{\frac{\hat{z}^2(t-\tau)}{\bar{p}_1^{\,2}(t)+\Sigma_{11}(t)}} \tag{2.36}$$

$$W_d(t-\tau) = \hat{z}^2(t-\tau)/\alpha(t-\tau) \tag{2.37}$$

By not allowing τ_c to increase any faster than real-time t, the model avoids sharp increases in $W_d(t)$ that could accompany changes in α. No limit on how fast τ_c decreases is necessary. Thus,

$$-\infty < d\tau_c/dt < 1 \tag{2.38}$$

2.4 Model vs. Data Comparisons

Using Eq. (2.36) for $\alpha(t)$, the OCM can be applied in a straightforward manner to predict tracking error statistics. It is necessary only to specify the parameter set Ω. Nominal settings used in this effort were

$\tau = .2$ sec, $\rho_{yi} = .01$ (i.e. -20dB)

$\tau_n = .1$ sec, $\rho_u = .01$ (i.e. -20dB)

$a_1 = 1.6$ deg, $a_2 = .8$ deg/sec, $a_3 = 3$ deg/sec

With a value of β=.707 in Eq. (2.36), the model mean tracking errors, $\bar{e}(t)$, showed greater lag-induced asymmetry trends than did the data. This indicates that $\beta = .707$, as suggested by heuristic arguements, generates values of $\alpha(t)$ that are too large. But, as the shape of the $\bar{e}(t)$ time-history correlates strongly with $z(t)$, it is not difficult to adjust β downward to bring model and data results into close agreement. We have found a suitable value to be

$$\beta_{Az} = \beta_{EL} = .41$$

which gives $C_\theta = .7$ or .3 in Eq. (2.25), depending on the sign of $\ddot{\theta}\theta$. Below we give model-data comparisons for the cases of shared and full attention with and without image visual cues. The data used for this study is that from our previous work in Reference [7].

2.4.1 Attention Sharing

The model vs. data comparisons are shown in Fig. 3a-b for azimuth axis tracking, and in Fig. 4a-b for elevation axis tracking. N=42 runs were used for obtaining these statistics. The results are in excellent agreement for both axes. This is most noteworthy considering the various complex issues such as interaxis attention allocation, image cues etc., that have been modeled and which have impact on the task. Moreover, this model-data agreement is of a quality not previously obtainable, especially for the elevation axis statistics.

Slight (< .5 deg) data-model mismatches can be adjusted by small changes in model parameters. However, it was not our intent to fine-tune model parameters here. Our interest was in model development/refinement so that a nominal (off-the-shelf) set of model parameters was used throughout.

Figure 5a shows the time-histories of $\alpha(t)$ that were generated by Eq. (2.36).

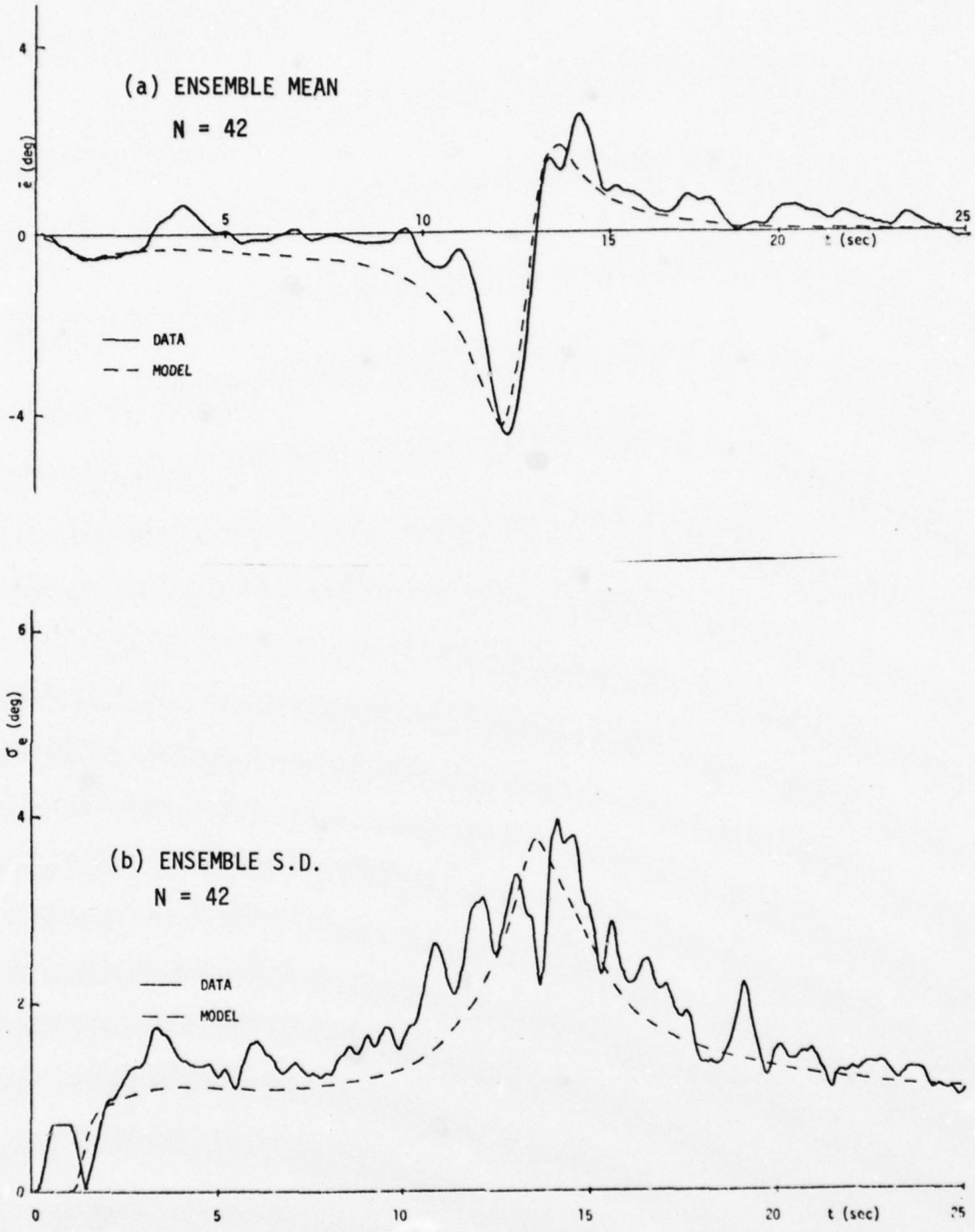

Fig. 3: AZIMUTH TRACKING ERRORS, SHARED ATTENTION, IMAGE CUES

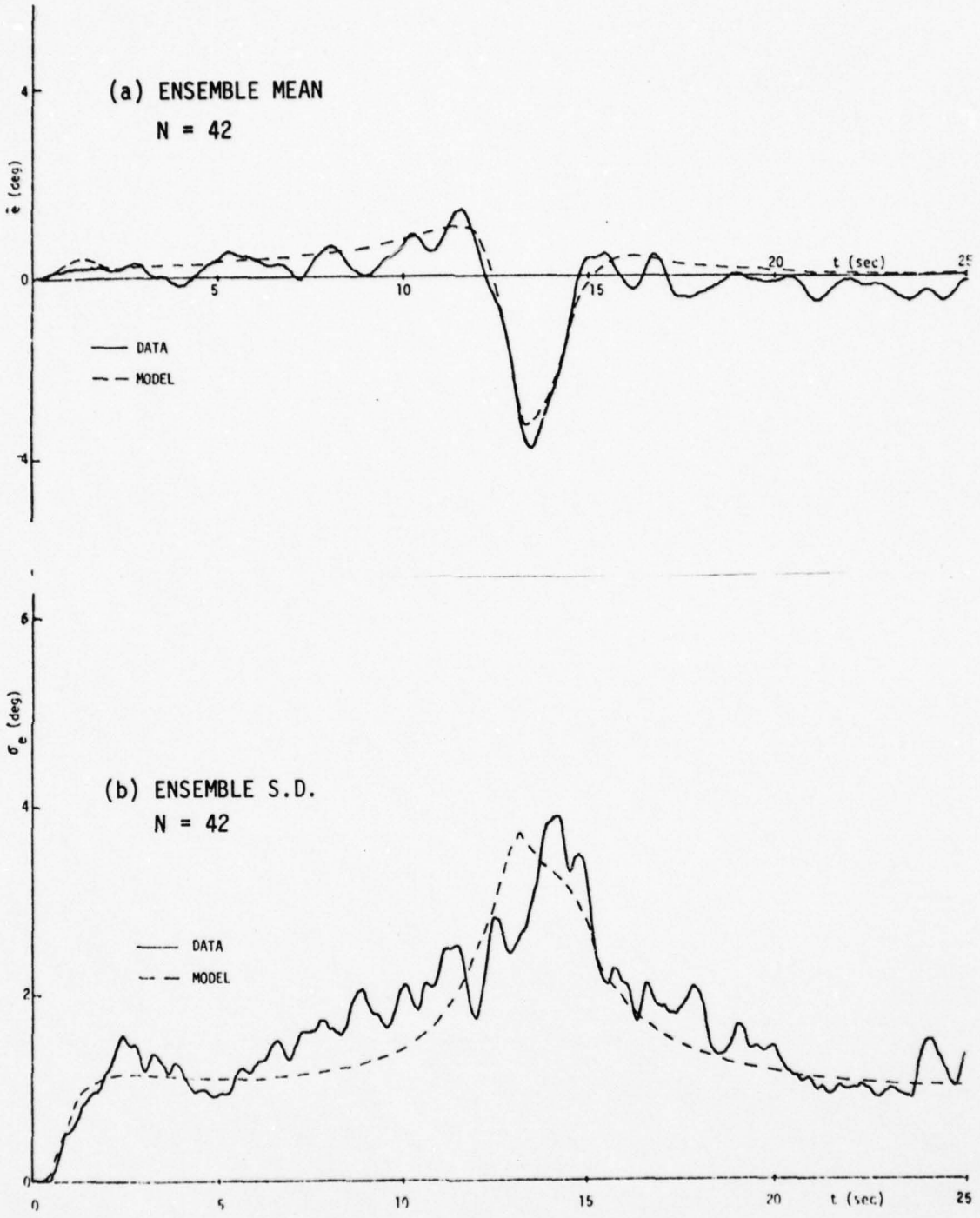

Fig. 4: ELEVATION TRACKING ERRORS, SHARED ATTENTION, IMAGE CUES

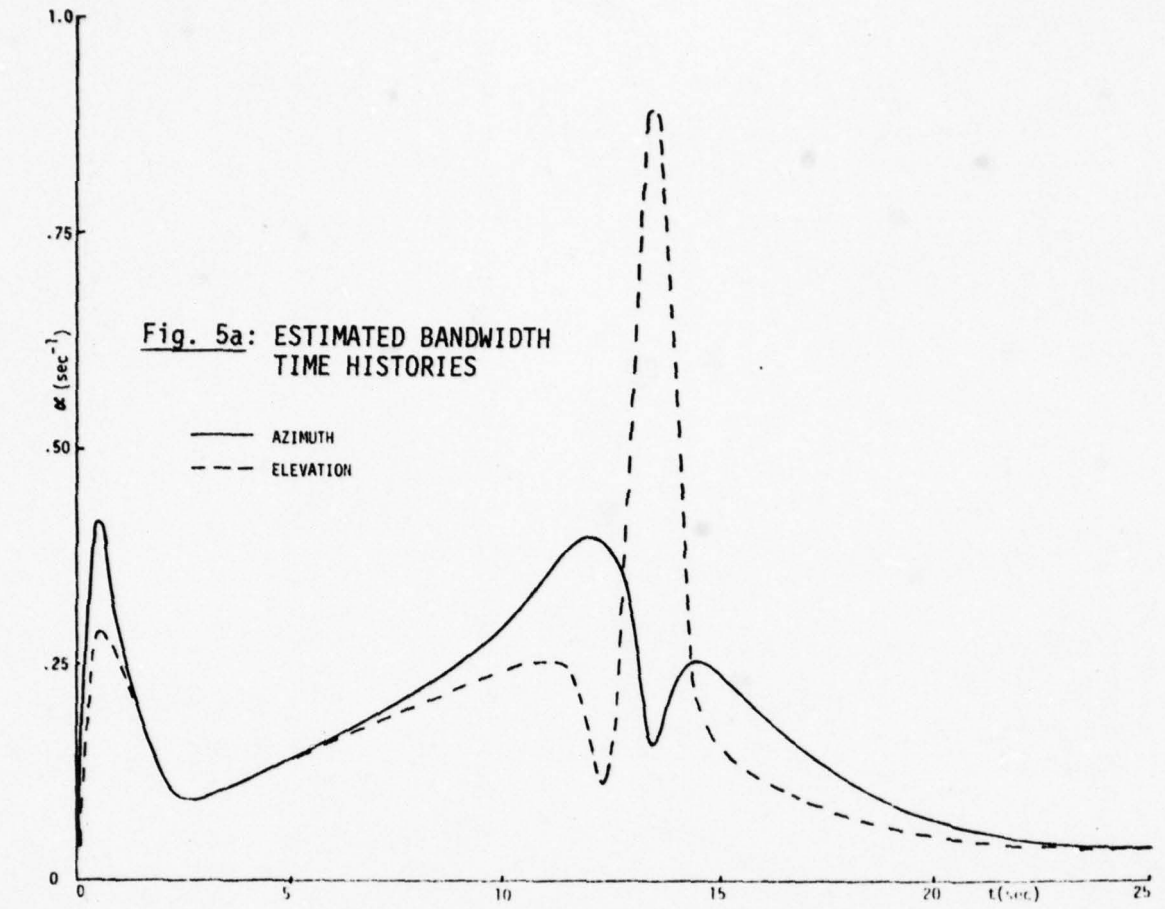

Fig. 5a: ESTIMATED BANDWIDTH TIME HISTORIES

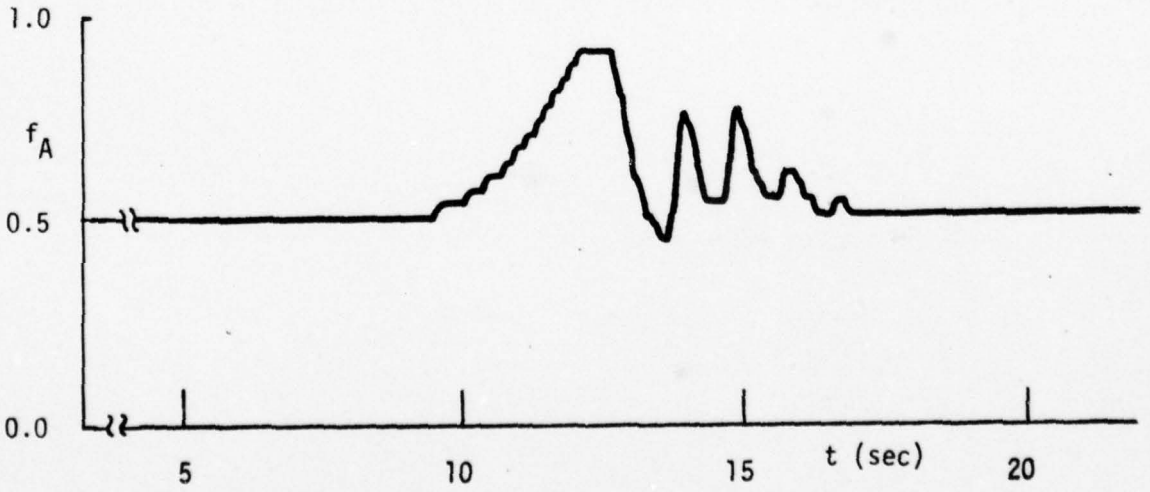

Fig. 5b: ATTENTIONAL ALLOCATION TO AZIMUTH AXIS TRACKING TASK

In azimuth, $\alpha(t)$ is bigger before crossover than it is after crossover as expected. Also note that $\alpha(t)$ for elevation is quite small, except during crossover. The large, sudden "pulse" in $\alpha(t)$ as $\dot{\theta}(t)$ goes through zero is what gives rise to the sharp (-4 deg) decrease in $\bar{e}(t)$ in Fig. 4a. The previous model structure in Ref. [7] could not produce this trend. The OCM prediction of attention allocation to the azimuth axis, $f_A(t)$, is shown in Fig. 5b. During most of the run attention is split 50:50, except that during the crossover period the bulk of the human's attention is on the azimuth axis.

When the target image is replaced by a triangular symbol of fixed size, no explicit information of $\dot{\theta}_T = y_3$ is assumed to be available in the model. With the removal of information, tracking error should increase. The model predicts a slight increase in $\bar{e}(t)$ for the azimuth axis (especially after crossover). The experimental results show a large increase in $\bar{e}(t)$ for this case, although model-data mean results are still within 2 standard errors. On the other hand the model predicts a significant increase in $\sigma_e(t)$ when the image cues are removed. The data match for this case is excellent (Fig. 6b), as the experimental results exhibit the same trend.

In the elevation axis the model predicts an increase in $\bar{e}(t)$, especially during the crossover period (Fig. 4a vs 7a). The data shows the same tendency and again model-data comparisons are excellent. On the other hand, the increased $\sigma_e(t)$ expected by the model, especially during crossover, is not apparent in the data. The values of $\sigma_e(t)$ increase only slightly over the target cues case (Fig. 4b), but no significant increase is seen during crossover.

2.4.2 Full Attention Case

Experiments were conducted that would allow the human operator to devote full attention to either the azimuth or elevation axis tracking task. This was

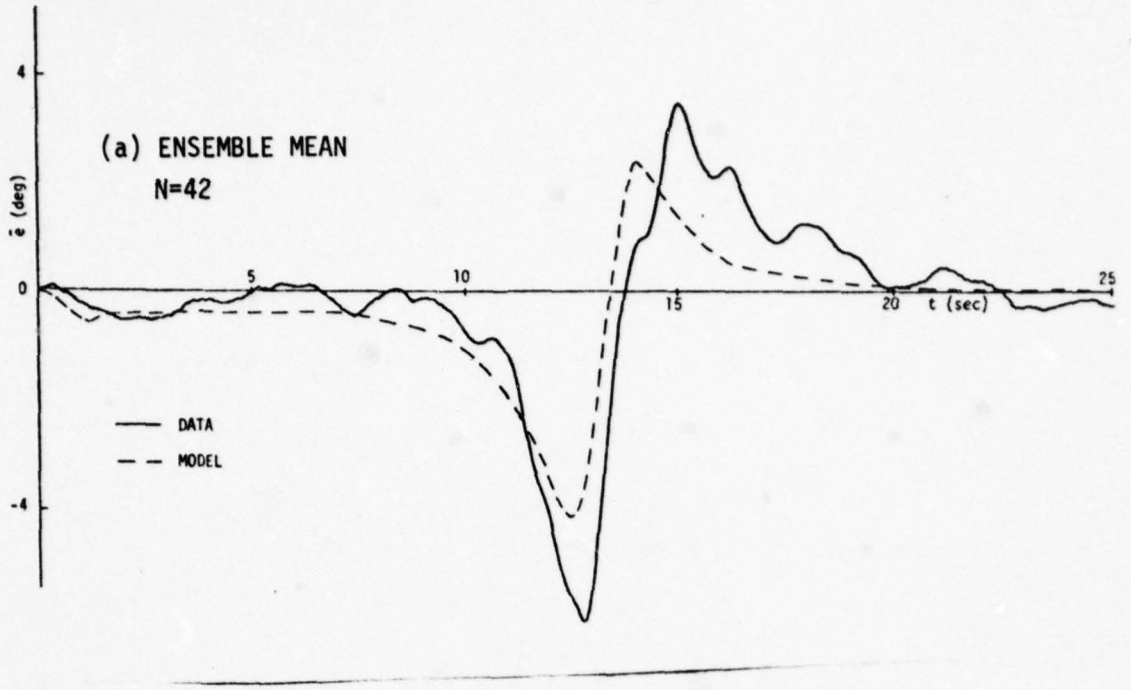

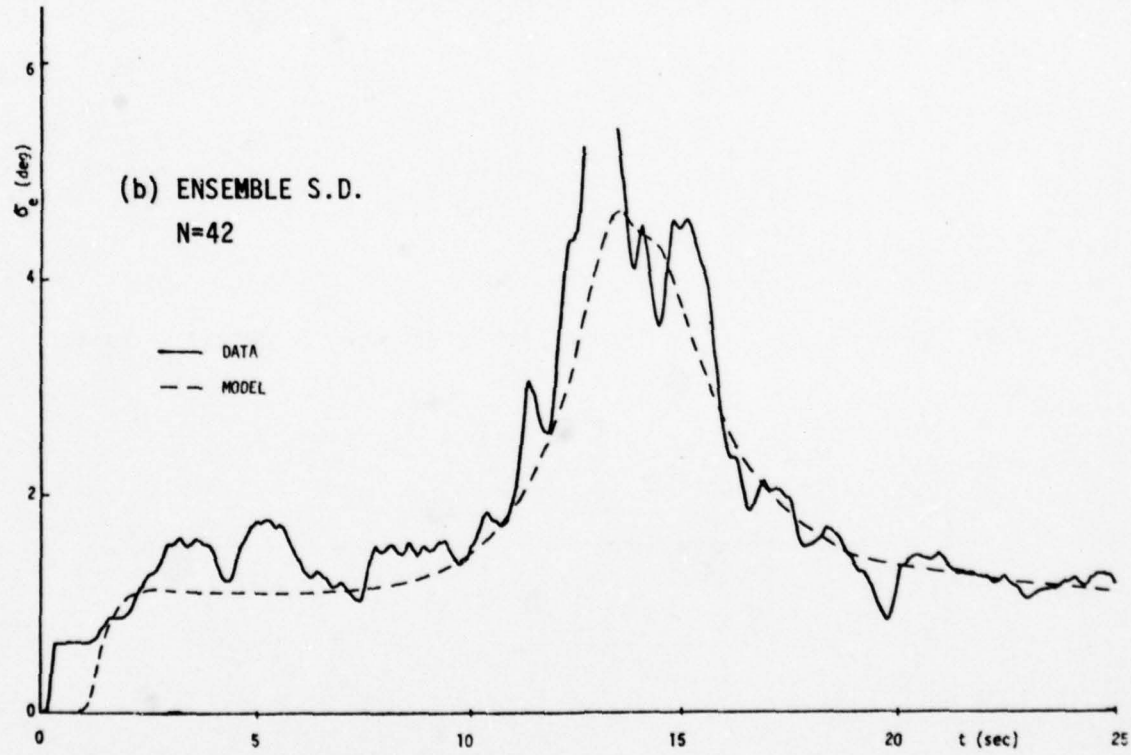

Fig. 6: AZIMUTH TRACKING ERRORS, SHARED ATTENTION, NO IMAGE CUES

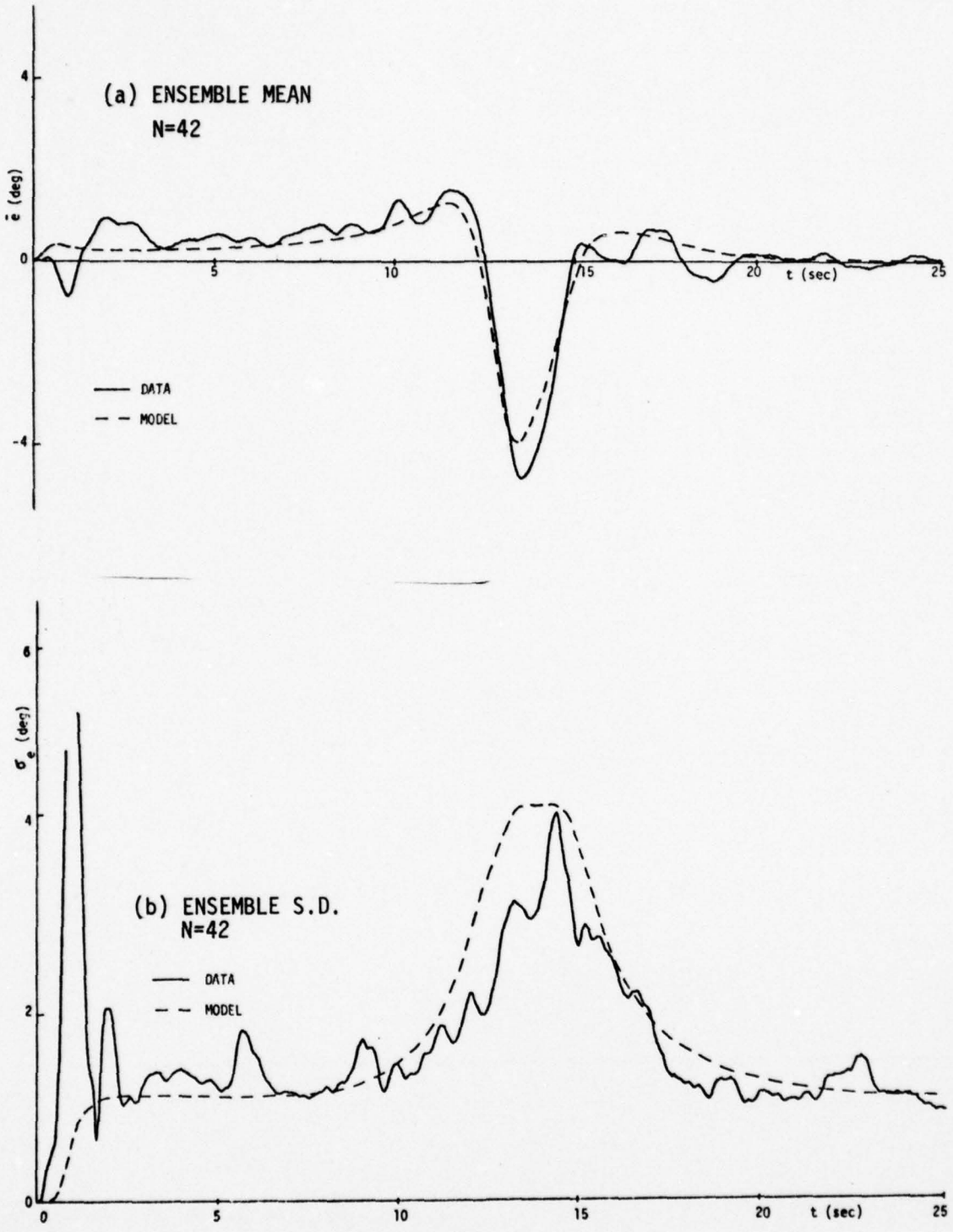

Fig. 7: ELEVATION TRACKING ERRORS, SHARED ATTENTION, NO IMAGE CUES

accomplished by clamping the error to zero in the other axis. Thus these experiments were designed to study the performance decrement associated with attention sharing in a two-axis single-operator tracking loop. For each condition N=18 runs formed the ensemble.

The modeling of this situation, where the human (supposedly) devotes full attention to the task, is readily accomplished by setting f_A or f_E to 1.0 as the case may be. As in the previous case, we model the removal of target image cues by dropping the observation of $\dot{\theta}_T = y_3$ from the model. The comparisons of model-vs-data tracking error statistics are shown in Figs. 8-11 for both azimuth and elevation axes.

For the case of target image cues (NY=3) the model prediction of $\bar{e}(t)$ in azimuth (Fig. 8a) is virtually identical to its shared attention counterpart (Fig. 3a), the only difference being a slightly larger peak lag at $t \simeq 12.5$. The closeness of these results comes from the fact that attention sharing in the vicinity of crossover places most attention on the azimuth task anyway (see Fig. 5b). The data seems to verify the similarity in $\bar{e}(t)$ for these two cases. On the other hand, $\sigma_e(t)$ is predicted to decrease by $\simeq .5$ deg from cross-over region onward for the full attention case. Figures 3 b and 8b show that the decrease in $\sigma_e(t)$ is well-captured in the model-data comparisons. Slight mismatches in $\sigma_e(t)$ for $0 \leq t \leq 10$ could be accounted for by a larger error threshold value, a_1.

The model-vs-data comparisons for the elevation axis (Fig. 4 vs Fig. 9) show a perplexing trend. The model predicts a decrease in the maximum $\bar{e}(t)$ overshoot at $t \simeq 13$ sec, as full attention is placed on the elevation task. The data shows a reverse tendency! The model predicts a decrease in $\sigma_e(t)$ that is significant in the $12 \leq t \leq 15$ sec crossover region, and somewhat less elsewhere. The data

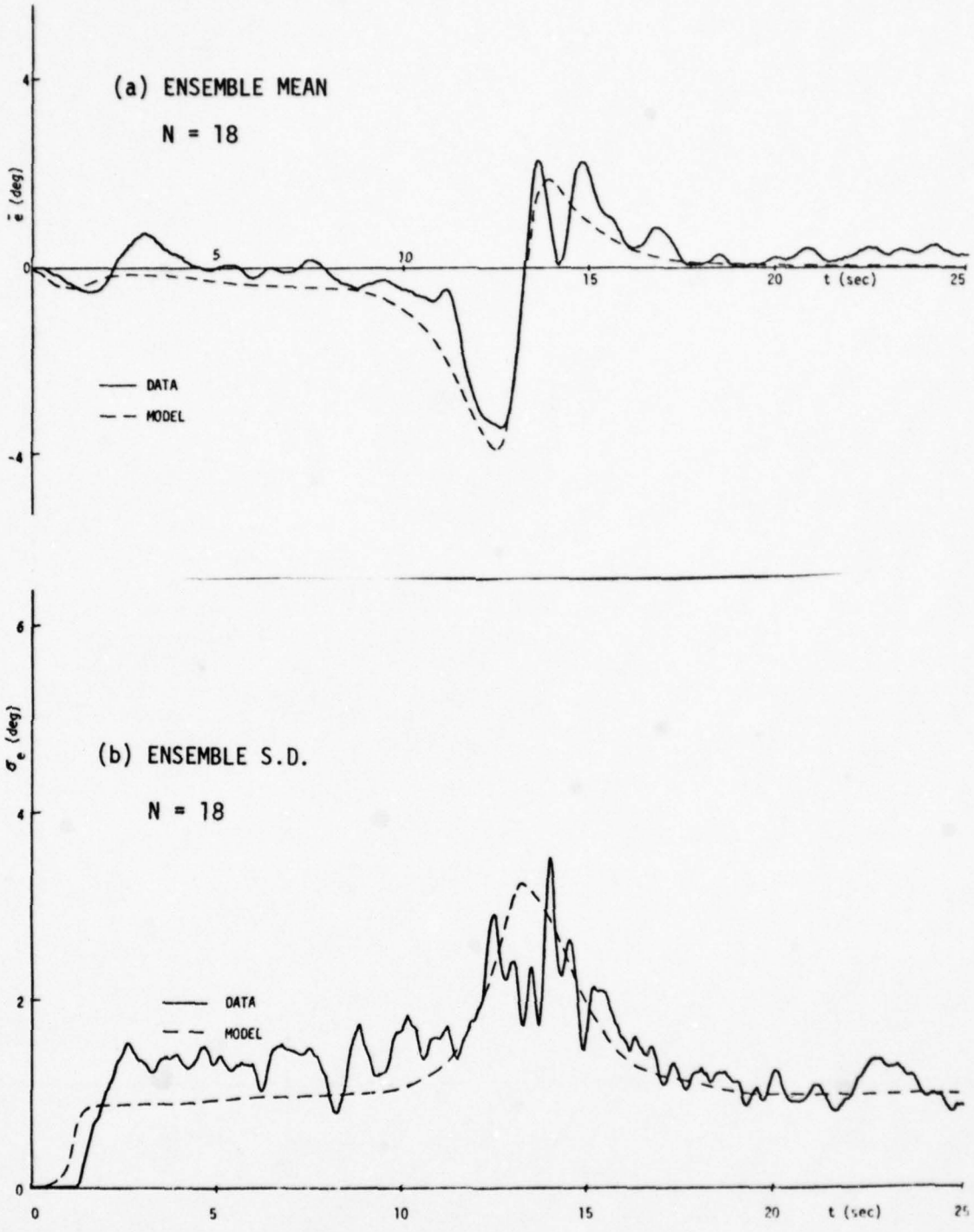

Fig. 8: AZIMUTH TRACKING ERRORS, FULL ATTENTION, IMAGE CUES

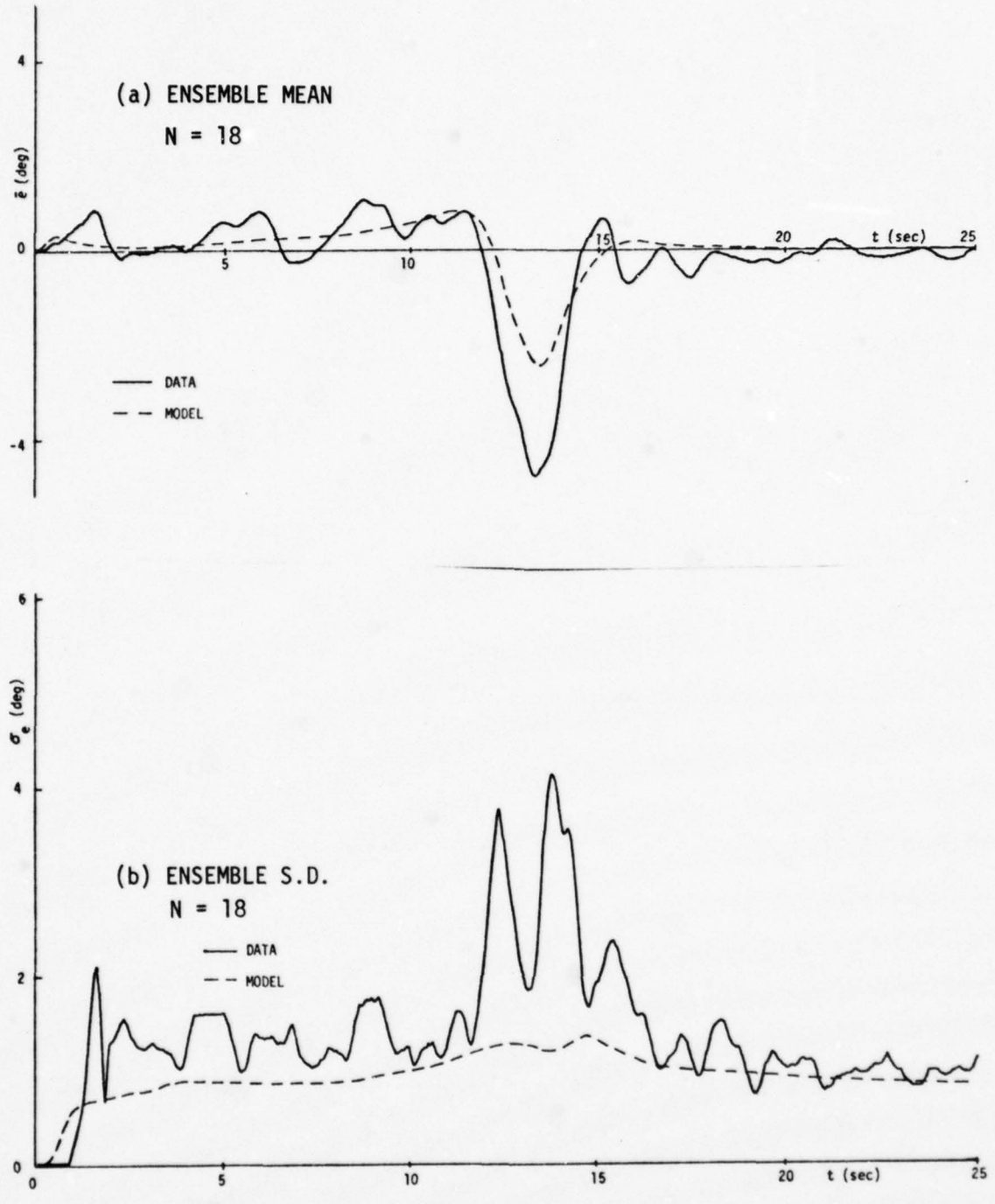

Fig. 9: ELEVATION TRACKING ERRORS, FULL ATTENTION, IMAGE CUES

does reflect a decrease in $\sigma_e(t)$ although it is difficult to draw a conclusion concerning $\sigma_e(t)$ in the crossover region. However, during the pre-and post-crossover regions of "good" tracking the decrease in $\sigma_e(t)$ data is more apparent.

When the target image is a triangle of fixed size and shape, no image cues are assumed (NY=2), and we obtain the data vs. model comparisons of Figs. 10-11. The model predicts very slight increases in $\bar{e}(t)$ and $\sigma_e(t)$ for azimuth tracking when the target visual cues are removed (compare Figs. 8 and 10). The data shows $\bar{e}(t)$ to increase in magnitude more so than predicted, yet the experimental values of $\sigma_e(t)$ hardly show a change between the two conditions. The model predictions for elevation tracking (Fig. 11) also show only slight increases over their NY=3 counterparts in Fig. 9. The data shows $\bar{e}(t)$ to be virtually unchanged between the two cases, although still larger than model predictions for $12.5 \leq t \leq 15$ sec. The experimental $\sigma_e(t)$ appears to have decreased (!) slightly and now agrees quite well with the model except for a sudden sharp peak between $13.5 \leq t \leq 15$ sec.

Comparing Figs. (6-7) with Figs. (10-11) shows the effect that inter-axis attentional allocation has on the tracking results when NY=2. The model predicts very little difference in azimuth $\bar{e}(t)$ for shared attention vs. full attention, wheras the data shows smaller $\bar{e}(t)$ for the later case. On the other hand model predictions of decreased $\sigma_e(t)$ for the full attention case correspond quite well with the data trends (Fig. 6b vs. Fig. 10b). In the elevation axis the model does predict a decrease in peak $\bar{e}(t)$ -- a trend is not seen in the data. But the relative changes in $\sigma_e(t)$ are captured quite well by the OCM (Fig. 7b vs. Fig. 11b).

2.4.3 Summary

When taken in total, the model data comparisons for the 16 cases studied are excellent. To be sure there are some discrepancies, as in the elevation axes for NY=2 with full attention. However, the mismatches are not major, occur almost invariably during crossover, and differences in means $\bar{e}(t)$ are usually less than

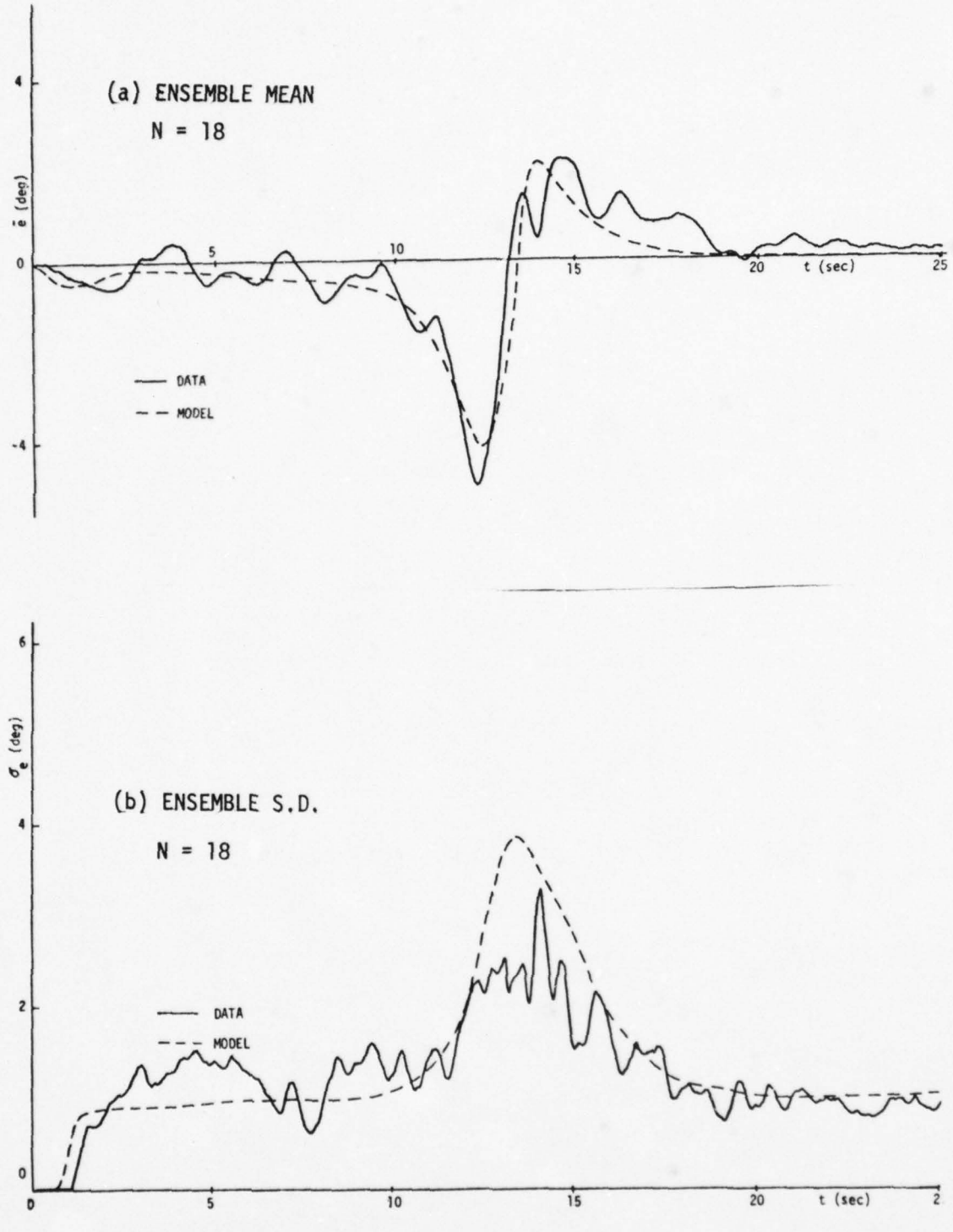

Fig. 10: AZIMUTH TRACKING ERRORS, FULL ATTENTION, NO IMAGE CUES

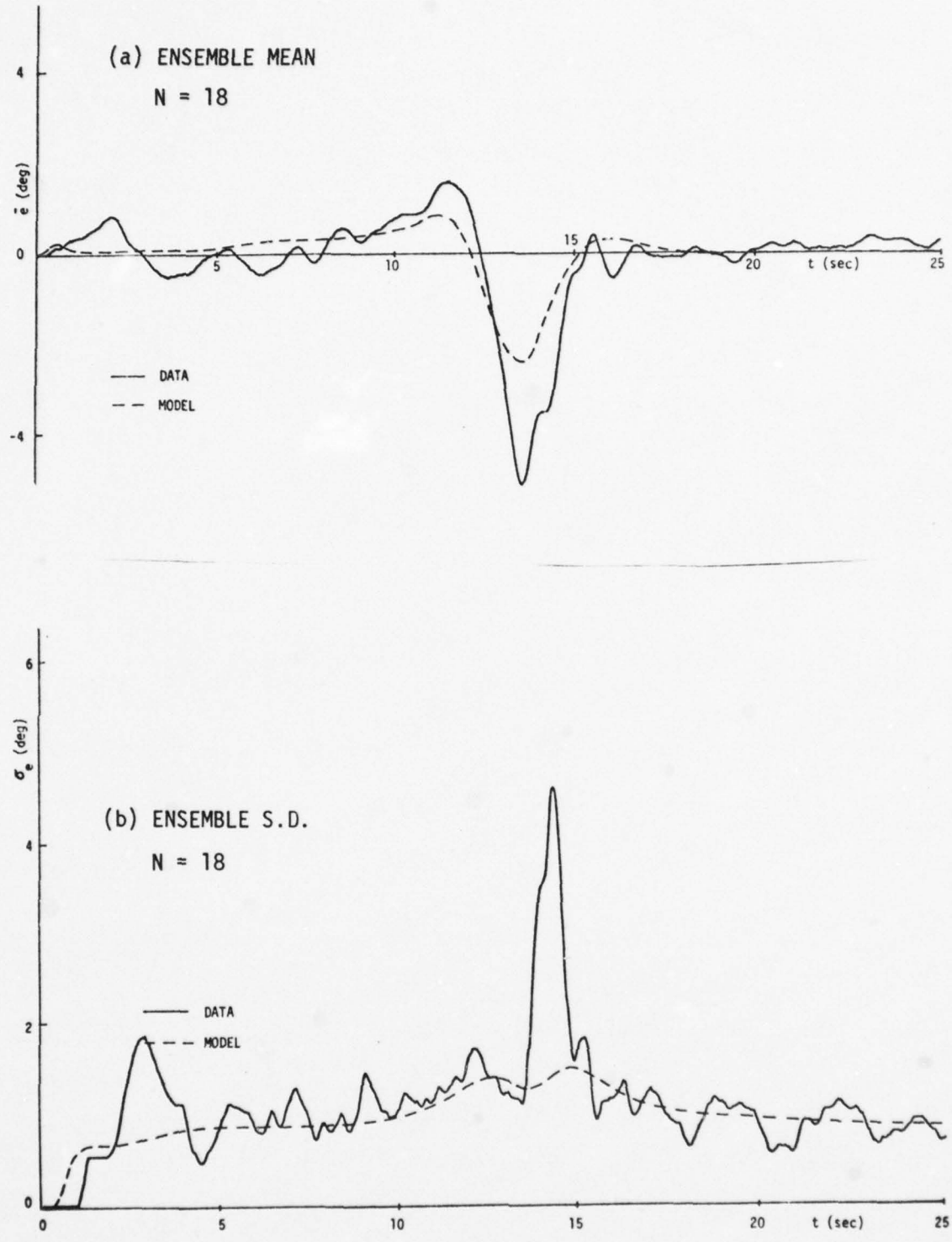

Fig. 11: ELEVATION TRACKING ERRORS, FULL ATTENTION, NO IMAGE CUES

2 standard errors $\sigma_e(t) / \sqrt{N-1}$. Model-predicted trends between the various cases generally agree with data. The use of a realistic target image for the shared attention case improves tracking performance as seen by comparing Figs. (3-4) with Figs. (6-7). On the other hand, the use of a target image for additional velocity cues has little effect in the full attention case. Going from shared attention to full attention on an axis improves tracking performance.

The major perplexities in model-vs-data mismatches occured in the full attention studies (Section 2.4.2). There are several reasons why these may have appeared:

1. Only N=18 runs made up the ensemble statistics for the full attention case, vs. N=42 for the shared attention case.
2. Training of the subjects was not as extensive as in the shared attention case.
3. The experimental mode of actually imposing full attention on an axis may not be achievable. The tracking task is somewhat artificial. Moreover, visual interference from the "clamped" axis may be a factor -- especially if the human (wrongly) expects motion in that axis.

III. TRACKING WITH INTERRUPTED OBSERVATIONS

In Chapter II an adaptive, first-order "internal" model of target angular velocity was quantified and included in the OCM to obtain a comprehensive manual tracking model. The resulting model was exercised in a dual-axis tracking task with realistic image cues and was found to give excellent model-vs.-data comparisons for both azimuth and elevation axes. This chapter describes a joint experimental/analytic study that provides additional justification of the "internal" model construct.

3.1 Introduction

Our approach to "internal" model verification involves the study of human tracking performance as modified by short periods (~1 sec) of target disappearance, or blanking. The blankings occur at pseudo-random times during a straight-and-level flyby. During the blanking period, the human's tracking response is governed almost entirely by his "internal" model representation of the target motion, as there is no visual information. Ensemble data from these experiments are used to suitably refine/validate the overall man-machine tracking model, including the target submodel.

The target blanking studies of this research are of considerable interest in related AAA tracking problems. Most research involving AAA tracking tasks has been done with continuously presented visual stimuli. This is not always realistic in practice. Visibility in the real world is rarely perfect and temporary target obscuration due to clouds, fog, optical/electronic countermeasures etc., is commonplace. Our analytic efforts represent an initial attempt at quantifying the effect of intermittent presentation of visual information on manual tracking performance.

The manual control literature lists a few experimental studies that were conducted to investigate the effects of temporary obscurations on tracking performance [17-19]. Gottsdanker [17] pioneered in the use of blanking experiments to study accuracy of predicted or extrapolated motion for +, -, and 0 accelerated motions. His results indicated that acceleration is not perceived directly, and that extrapolated motion attains a constant rate approximately 1-2 sec after blanking.† The existence of a rate-smoothing mechanism in tracking was hypothesized. These results were in qualitative agreement with the tendency of humans to lag (lead) an accelerating (decelerating) target. However, the data collected coarsely at 1 sec intervals is not suited for developing a quantitative model that would be applicable to the time period immediately following blanking.

Hammerton and Tickner [18] and Pew [19] used blanking experiments to determine the time required for a human to recover a target following a period of visual interruption. The qualitative results of these three earlier studies will be reconciled with the results of our analytic model.

3.2 Experimental Program

A set of tracking experiments was conducted to investigate transient phenomena and target acquisition modes via interrupted observations. In the experiments the subjects tracked manually a stylized delta-shaped aircraft image both in azimuth and elevation, using a two-axes control stick. At certain times during the 25.575-sec run the CRT screen was blanked for a period of 1-sec, that is, the target image disappeared from the screen. A straight-and-level, constant velocity, aircraft flyby (crossover range = 50 ft., altitude = 50 ft., velocity = 38.9 fps) was used in each of the following five experimental conditions:

---

†i.e., after a short transient the human becomes a constant-velocity extrapolator.

A: No blanking during the run

B: Blanking at 7.79 sec (5 sec before crossover, crossover=12.79 sec)

C: Blanking at 9.79 sec (3 sec before crossover)

D: Blanking at 13.79 sec (1 sec after crossover)

E: Blanking at 15.79 sec (3 sec after crossover)

Six subjects, all University of Connecticut ROTC students, participated in the study. The subjects were well-trained on our tracking simulator using a variety of simulated trajectories that did not include any blankings. In all cases the subjects tracked to minimize error, and were scored using a (total) RMS tracking error criterion. They were informed of their score following each run and were encouraged to keep it as low as possible.

In the data-taking runs each subject was presented with seven replications of each experimental condition, in randomized order. This type of experimental design, when aggregated across subjects yields statistics (central tendency and variance) that are indicative of the subjects' population. The source of randomness in this design is the inter-subject variability. This type of design has the added advantage of minimizing artifacts such as the effects of learning.

The data collected were the time-histories of tracking error, e(t) and human input, u(t), in azimuth and elevation. At a sampling rate of 40/sec., each run yielded 1024 datum points for each of the variables recorded. For the same experimental condition, the 42 (=6 subjects x 7 replications) time-histories were ensemble averaged to obtain mean tracking error ($\bar{e}$) and standard deviation (σ_e) vs time for both azimuth and elevation axes. The averaging process first was done for each subject and then across subjects to obtain the "grand" averages.

As expected, the ensemble statistics for condition A closely resembled the data reported in Chapter II and Ref. [7] for the case of shared attention and image visual cues. The most notable feature of this data is the asymmetry in mean

tracking error that initiated the research into internal models for target motion. The ensemble statistics for conditions C and D gave clear evidence of the blanking effects superimposed on the basic nonblanking error patterns. These deviations from the baseline condition A were tested using a point-by-point t-test and were found to be significant at .01 level of significance. However, the ensemble statistics for conditions B and E were not significantly different from the condition A at .01 level. Therefore, only the results of conditions A,C and D are presented and discussed in this chapter.

3.3 Analytic Modeling

In order to apply the OCM to predict tracking performance under blanking conditions, it is necessary to model the effects of blanking on the human operator's control and information processing functions. Our modeling approach is based on the following reasonable assumptions:

(i) the task objectives are expressed by the same quadratic cost functional during blanking and normal tracking periods;

(ii) the human adopts an optimal strategy, subject to his inherent limitations, during the entire run;

(iii) the observation noise, $\underline{v}_y(t)$ is assumed to be ∞ during blanking periods.

A consequence of assumptions (i) and (ii) is that the human's feedback control strategy is unaffected by blanking. This follows from a well-known result [20] that the optimal control policy is independent of the probability of visual interruption for a linear system with a quadratic cost functional. Thus, the controller portion of the OCM remains unchanged with blanking.

On the other hand, target blanking has direct impact on the human's information processing function, since the visual interruption degrades the quality of state estimates. The information processor of the OCM can be generalized to include the effects of target blanking. Recall that the Kalman filter estimate $\underline{p}(t)$ is given by

$$\dot{\underline{p}}(t) = A\,\underline{p}(t) + B\,\mu(t-\tau) + G(t)\,[\underline{y}_p(t) - C\,\underline{p}(t)] \tag{3.1}$$

Here $\mu(\cdot)$ is the deterministic control input, $\underline{y}_p(t)$ is the perceived output and $G(t)$ is the filter gain given by

$$G(t) = \Sigma(t)\,C'\,V_y^{-1}(t-\tau) \tag{3.2}$$

where $\Sigma(t)$ is generated from the Riccati equation

$$\dot{\Sigma} = A\,\Sigma + \Sigma\,A' - \Sigma\,C'\,V_y^{-1}(t-\tau)C\Sigma + \text{diag}\,[F_0 W_d F_0', V_u] \tag{3.3}$$

Here $V_u(\cdot)$ is the motor noise covariance and $W_d(t-\tau)$ is the pseudo-driving noise covariance matrix given by

$$W_d(t-\tau) = \hat{z}^2(t-\tau) \,/\, \alpha(t-\tau) \tag{3.4}$$

where

$$\alpha(t-\tau) = 0.41\sqrt{\frac{\hat{z}^2(t-\tau)}{\bar{p}_1^{\,2}(t) + \Sigma_{11}(t)}} \tag{3.5}$$

and $\hat{z}(t-\tau)$ is computed from filter innovations via the WLS algorithm of Chapter II. The diagonal elements of the observation noise covariance matrix $V_y(t)$ are

$$V_{yi}(t) = \frac{\pi\,\rho_{yi}}{r(t) f_i\, N_i^{\,2}}\; E\{y_i^{\,2}(t)\}\;;\; \rho_{yi} \sim .01 \tag{3.6}$$

Here f_i is the attention allocation to either azimuth or elevation axis given by Eq. (2.21) and N_i is the RIDF gain of a visual/indifference threshold of width $\pm\, a_i$.

In Eq. (3.6), $r(t)$ is the "blanking factor" that accounts for the effects of target blanking. Since it is assumed that $V_y(t) = \infty$ during blanking, the blanking factor, $r(t)$ is of the form

$$r(t) = \begin{cases} 1 \text{ during periods of normal tracking} \\ 0 \text{ during periods of blanking} \end{cases}$$

At issue then is how the 1-0 and 0-1 transitions should be effected. When the target is blanked we assume that all visual information suddenly ceases and that $r(t) \to 0$ instantaneously. On the other hand, experimental evidence suggests that following a period of visual interruption, there is a finite re-accommodation time. Hammerton and Tickner's [18] target blanking studies indicate $\simeq$ 1 sec to completely recover the target. Pew's [19] results indicate a delay of $\simeq$ 0.35 sec in response initiation. Based on this we bring r(t) from 0 to 1 exponentially with a time constant τ_b of 0.35 sec. The model results were found to be insensitive to the value of τ_b in the range 0.25 - 0.40 sec. This implies that the target recovery time of 1 sec, which corresponds to 2.5 to 4 time constants, τ_b, is an appropriate number. The blanking factor, r(t), for the case when blanking occurs between times t_1 and t_2 is given by

$$r(t) = \begin{cases} 1.0 \; ; \; t < t_1 \\ 0.0 \; ; \; t_1 \leq t \leq t_2 \\ 1 - \exp\left[-(t-t_2)/\tau_b\right] \; ; \; t \geq t_2, \; \tau_b = 0.35 \text{ sec.} \end{cases} \tag{3.7}$$

Modification of $V_y(t)$, via the blanking factor, r(t), is the <u>only</u> change required to model blanking conditions using the OCM. Since the observation noise $V_y(t) = \infty$ during blanking, the filter gain G(t) of Eq. (3.2) is zero. This implies that the evolution of $\Sigma(t)$ of Eq. (3.3) would be governed almost entirely by the internal model parameters. In particular, the filter estimate of angular velocity, $p_1(t) = E\{\dot{\theta}_T(t-\tau)/y_p(\sigma), \; \sigma \leq t\}$ <u>during blanking</u> is given by

$$\dot{p}_1(t) = -\alpha(t-\tau) \; p_1(t) \tag{3.8}$$

Therefore, it is clear that the internal model parameter, $\alpha(t-\tau)$ is the major quantity that affects tracking performance and the results of blanking experiments should help verify the internal model construct.

The process of generating $\hat{z}(t-\tau)$ follows the usual WLS algorithm of Chapter II and the internal model parameter, $\alpha(t-\tau)$ is still given by Eq. (3.5). These quantities evolve in time, as in no blanking case, driven by the Kalman filter outputs. However, as $V_y(t) \to \infty$, rapid changes occur in key model elements. Specifically, Σ_{11} increases monotonically with increased blanking time, since there is no feedback from visual observations. This implies, as can be seen from Eq. (3.5), that $\alpha(t-\tau) \to 0$ with increased blanking time. This results in a constant $p_1(t)$, the Kalman filter estimate of angular velocity, as is evident from Eq. (3.8). The last item is consistent with the experimental findings of constant velocity extrapolations after 1-2 sec [17].

3.4 Model vs Data Comparisons

With the generalization of section 3.3 included in the OCM, prediction of tracking error statistics for the blanking and no blanking conditions is straightforward. It is only necessary to specify the parameter set

$$\Omega = \{\tau, \rho_u, \tau_n, a_i, \rho_{yi}\}$$

Nominal settings used in this effort were

$$\begin{aligned} \tau &= 0.2 \text{ sec}, & \rho_{yi} &= 0.01 \text{ (i.e. -20 db)} \\ \tau_n &= 0.1 \text{ sec}, & \rho_u &= 0.01 \text{ (i.e. -20 db)} \\ a_1 &= 1.6 \text{ deg}, & a_2 &= 0.8 \text{ deg/sec}, \; a_3 = 3 \text{ deg/sec} \end{aligned} \tag{3.9}$$

The internal model parameter, α was computed via Eq. (3.5). On the basis of previous discussions the recovery time constant, τ_b, associated with the "blanking factor", r(t), was set at 0.35.

3.4.1 No Blanking Case

The model vs data comparisons for azimuth axis tracking with no blanking (condition A) are shown in Fig. 12a-b. The major data characteristics are replicated quite well. In particular, the asymmetry in the mean tracking error profile is reproduced by the model via the internal model parameter, α. The slight lagging

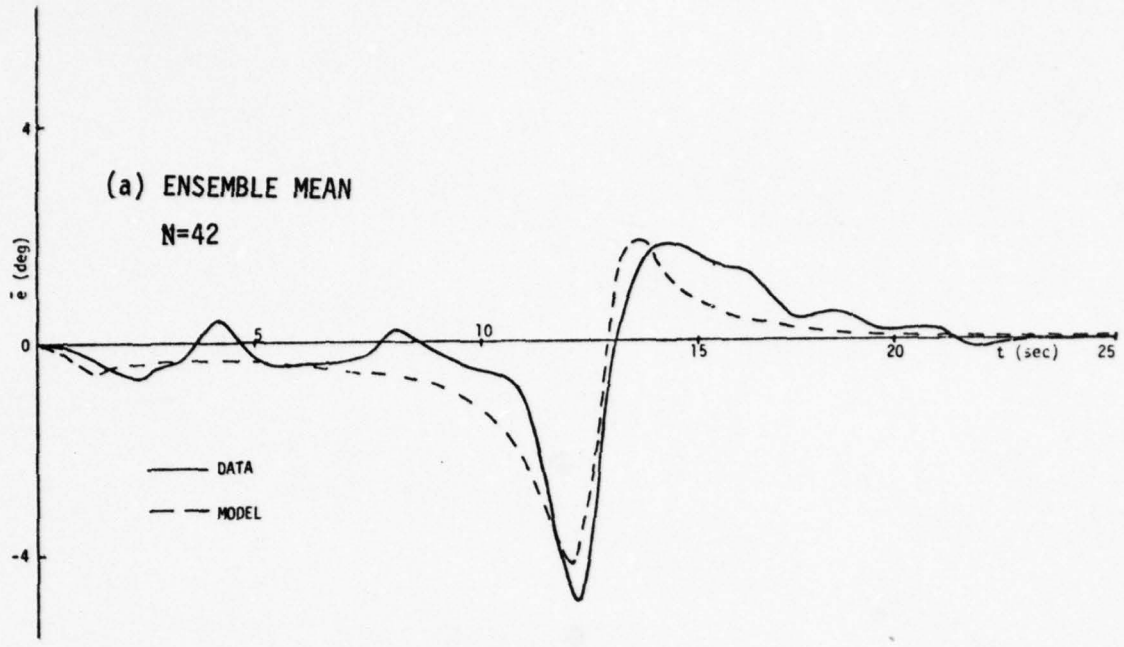

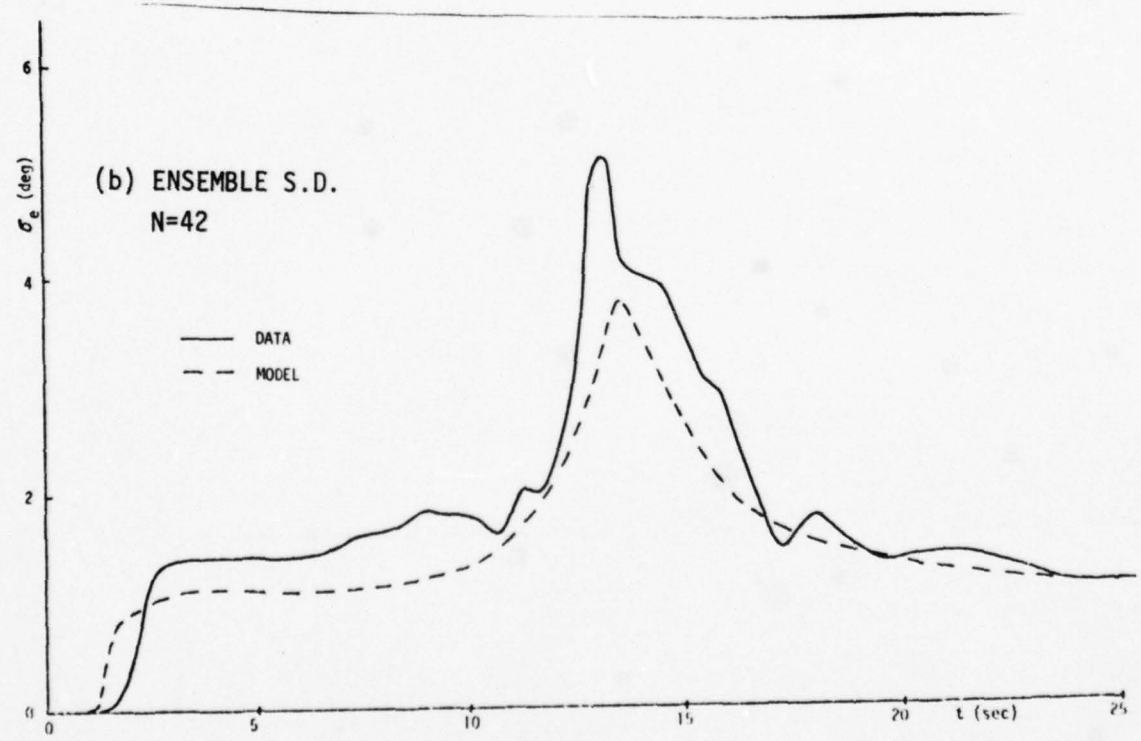

Fig. 12: AZIMUTH AXIS TRACKING, NO BLANKING CONDITION

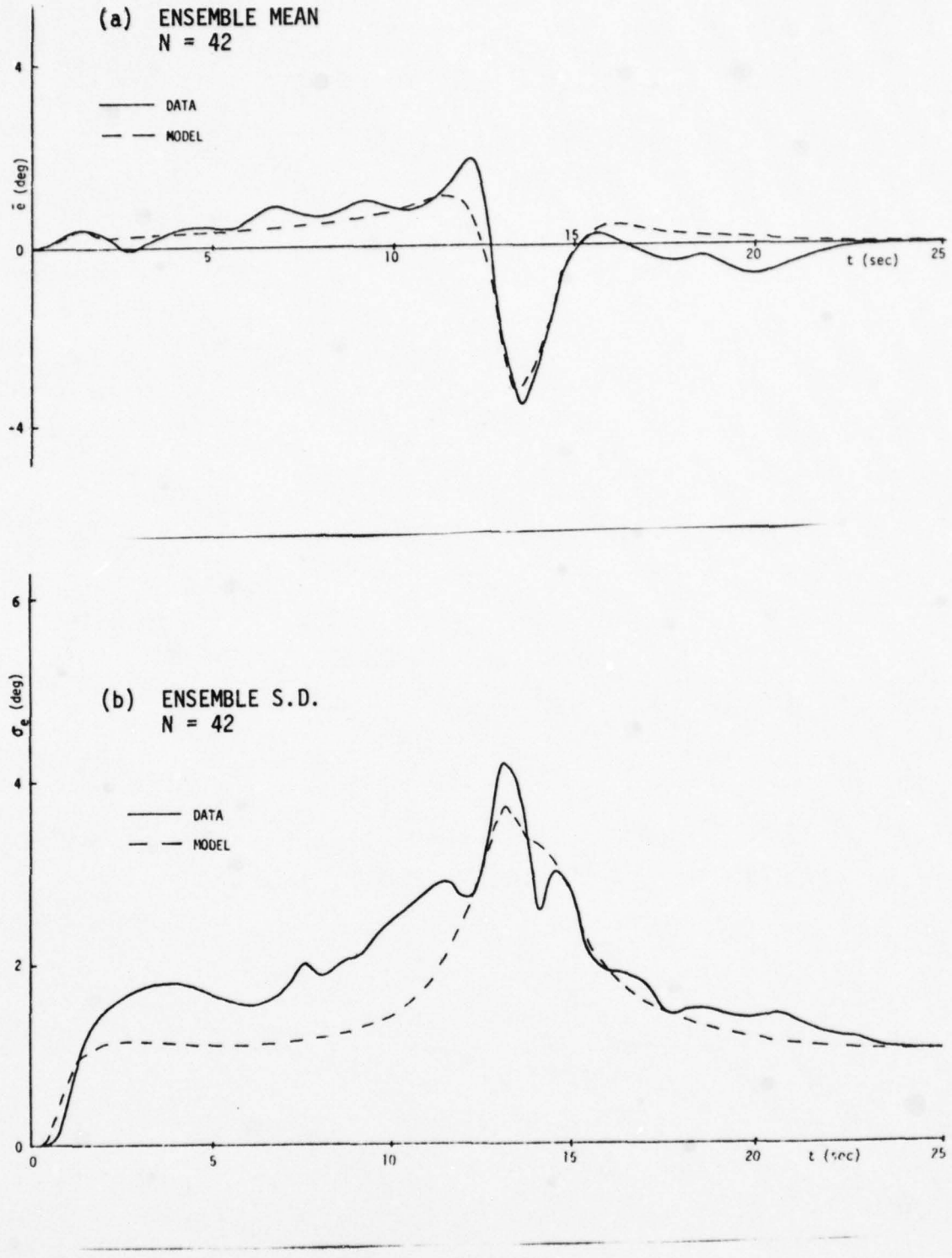

Fig. 13: ELEVATION AXIS TRACKING, NO BLANKING CONDITION

tendency in the mean tracking error for $0<t<4$ (Fig. 12a) and the large standard deviations, σ_e (1.0-1.5 deg) during periods of good mean tracking (Fig. 12b) are also replicated. These data aberrations were attributed to the choice of small display gain, $k_d \simeq 1/9$, which in turn, resulted in large visual/indifference thresholds, a_i in the OCM [7]. The minor mismatch in σ_e for azimuth tracking during the crossover period (Fig. 12b) can be adjusted by a 1 db increase in ρ_y, with no noticeable effect on the model vs data comparisons for $\bar{e}(t)$. However, it was not our intent to fine-tune model parameters here. Our intent was in model development/refinement so that the nominal set of model parameters of Eq. (3.9) was used throughout.

The model vs data comparisons for elevation axis tracking with no blanking (condition A) are shown in Fig. 13a-b. The model-data agreement is also very good, especially for $\bar{e}(t)$. The observed differences in σ_e, for $1<t<6$ (Fig. 13b) can be accounted for by visual/indifference thresholds that decrease as the run progresses. *This data aberration is not seen in any other tracking response [5,7].* It could be an artifact of training or pre-conditioning, and no attempt was made to model it further.

The good model-data agreement for both axes under condition A is most noteworthy considering the various complex issues such as interaxis attention allocation, image cues, etc. that have impact on the task.

3.4.2 Blanking After Crossover (Condition D)

Fig. 14 shows the time-histories of $\alpha(t)$, generated using Eq. (3.5), for the case when blanking occured at 13.79 sec (1 sec after crossover). As expected from the theory, $\alpha(t)$ monotonically decreases during blanking. Following the period of visual interruption, $\alpha(t)$ exhibits a peaked transient. This should also be expected in view of rapid decrease in Σ_{11} with the return of visual information. The same trend is exhibited by $\alpha(t)$ for the case when blanking occured prior to

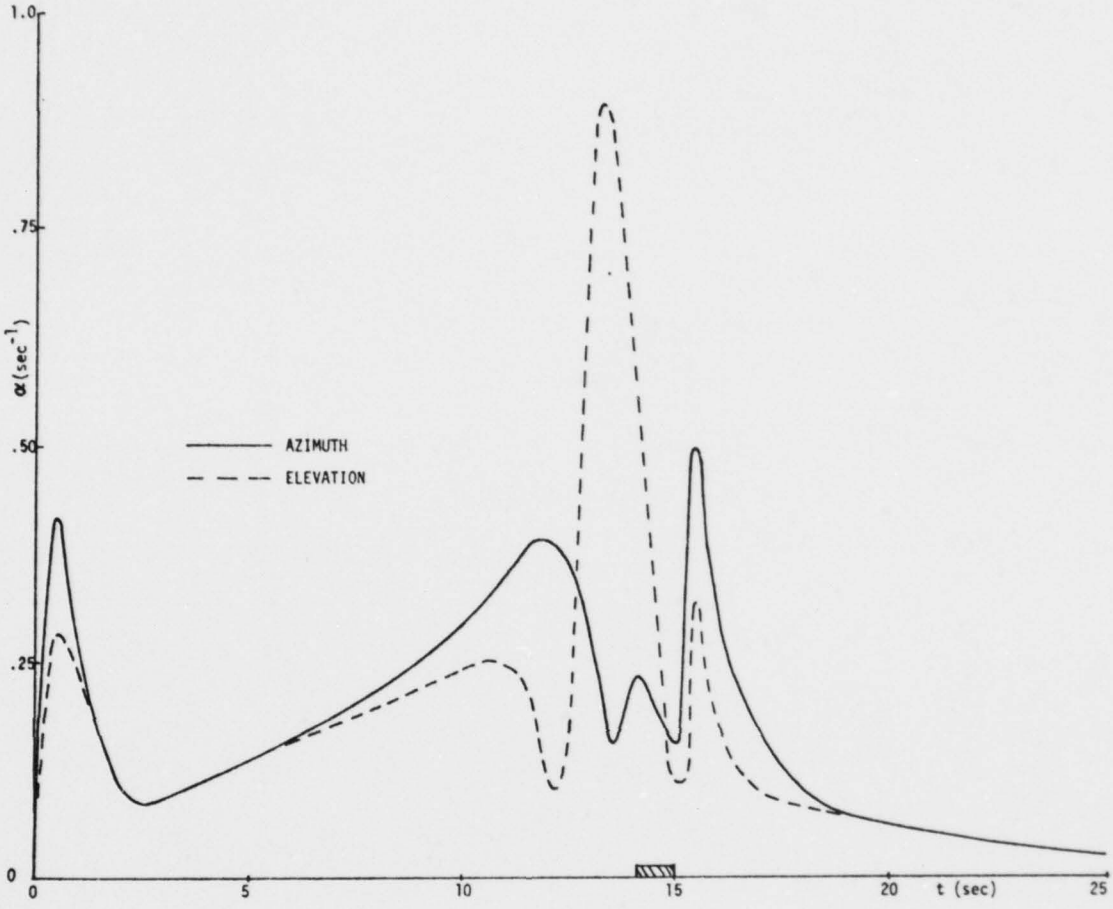

Fig. 14: ESTIMATED BANDWIDTH TIME HISTORIES SHOWING EFFECT OF TARGET BLANKING

crossover, although the results are not shown here.

Since $\alpha(t)$ decreases monotonically towards zero with extended periods of blanking, one could argue that the good model-data comparisons for the non-blanking condition may be fortuitous and that the previous model structure with $\alpha = 0$ and a constant correlation time, τ_c for $\ddot{\theta}(t)$ may still be appropriate. To clarify this issue, the model as it existed prior to the present study [3,5] with $\alpha = 0$ and $\tau_c = 0.5$ was applied to this case of post crossover blanking at 13.79 sec. (condition D). The results for azimuth axis tracking, shown in Fig. 15a-b, clearly indicate the inadequacy of the previous model structure: predicted mean errors are of an order of magnitude larger than the data (see Fig. 16) and the standard deviations are substantially smaller than the experimental results.

The new model/data comparisons for azimuth axis tracking with blanking at 13.79 sec (condition D) are shown in Fig. 16a-b. The sudden increases in $\bar{e}(t)$ and $\sigma_e(t)$ indicate a high sensitivity to the loss of visual information for this blanking case. This can be attributed to a large angular acceleration, $\ddot{\theta}(t)$ - 22 deg/sec^2 at the time of blanking, which makes the prediction/extrapolation of target position a difficult task. The model captures these data trends qualitatively and quantitatively. The model also duplicates quite accurately the recovery transient following the return of visual information.

The model vs data elevation axis results for condition D are shown in Fig. 17a-b. There is one notable data aberration in Fig. 17a: the data prior to blanking time does not agree with the no blanking data (Fig. 12a). Non-causal behavior aside, this should not occur as the experimental runs were randomized. It could indicate that N=42 runs is not sufficient for statistical purposes. However, the model-data mismatches in Fig. 17a are within experimental/inter-subject variability. On the other hand, the experimental standard deviations $\sigma_e(t)$, shown in Fig. 17b, are replicated quite accurately by the model.

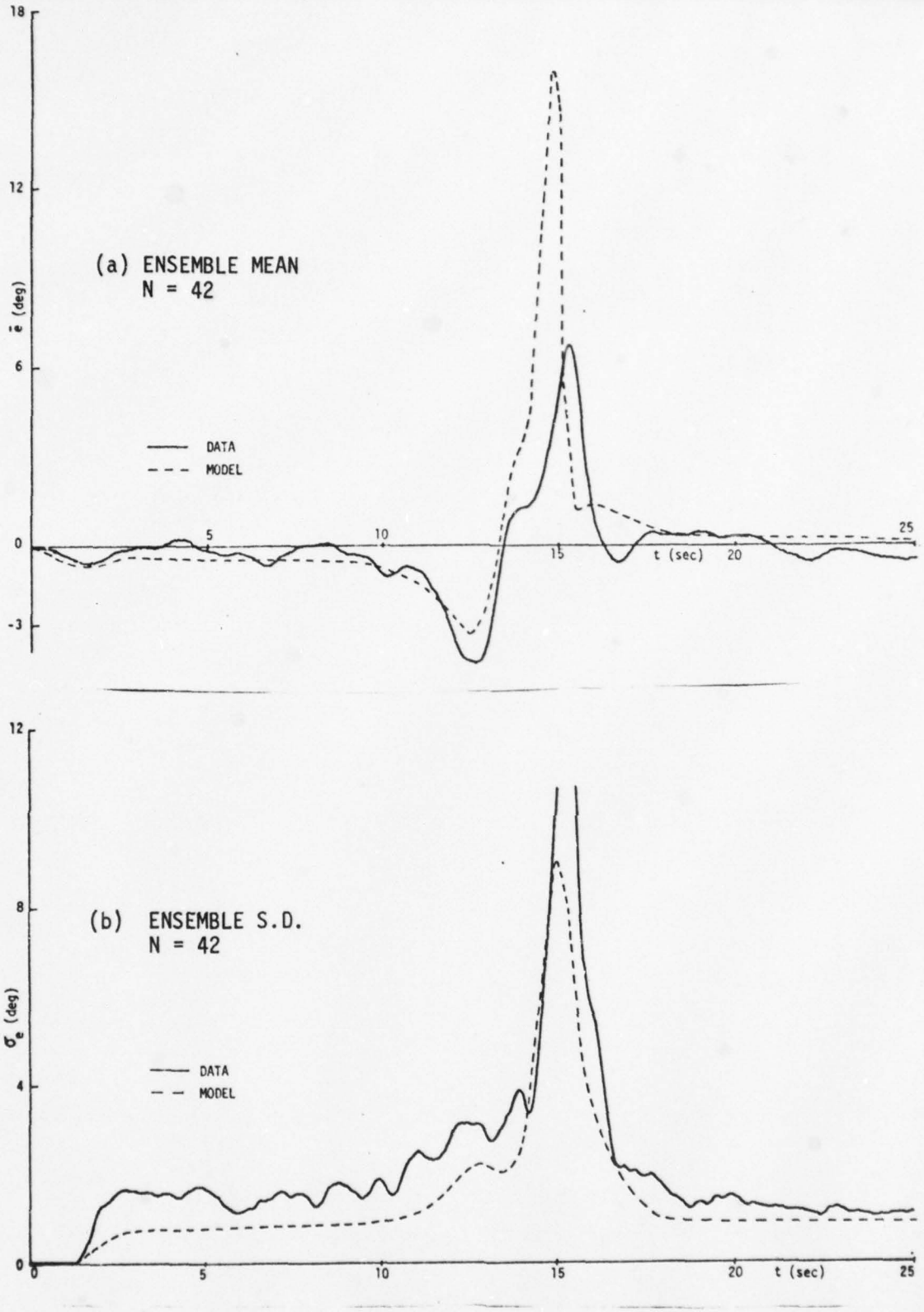

Fig. 15: AZIMUTH AXIS TRACKING, BLANKING AT t=13.79, OLD MODEL STRUCTURE

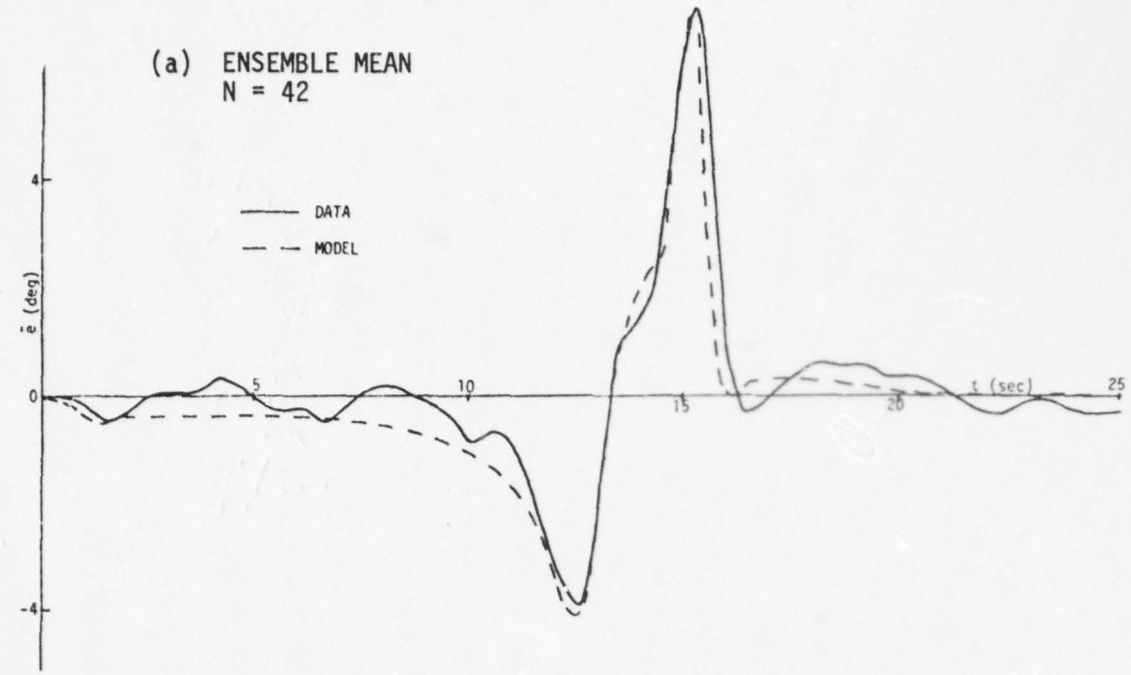

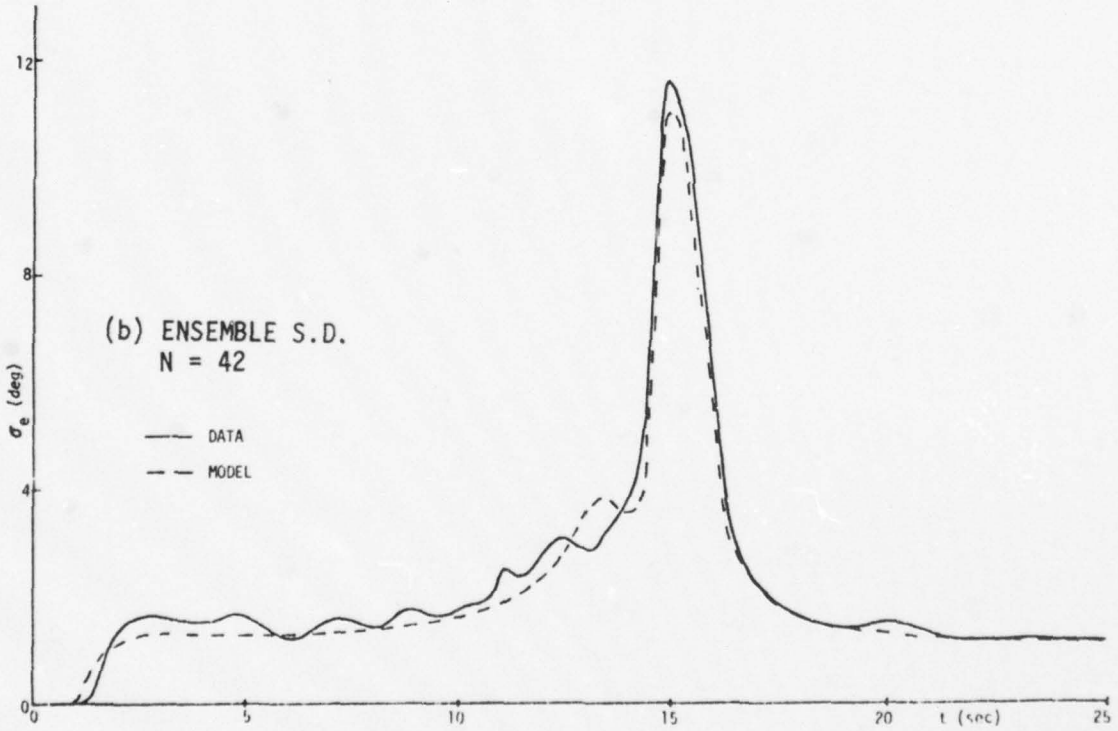

Fig. 16: AZIMUTH AXIS TRACKING, BLANKING AT t=13.79

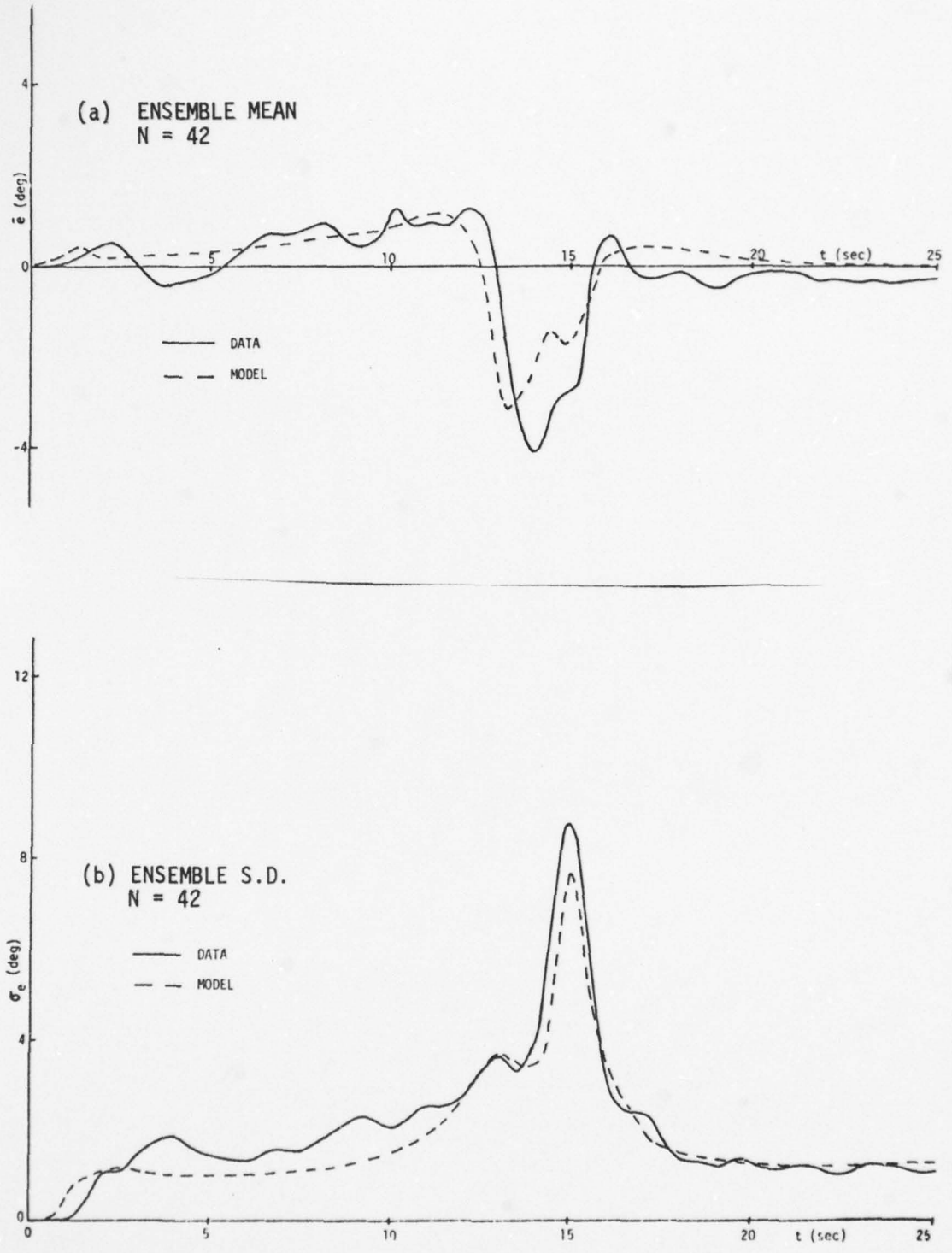

Fig. 17: ELEVATION AXIS TRACKING, BLANKING AT t=13.79

3.4.3 Blanking Prior to Crossover (Condition C)

The model vs data comparisons for azimuth axis tracking with blanking at 9.79 sec (condition C) are shown in Fig. 18a-b. Although structurally similar, the model predictions of $\bar{e}(t)$ exhibit greater lag than the experimental results during blanking. The model duplicates quite accurately the recovery transient following the target reappearance, however. We feel that the peak in σ_e (Fig. 18b) is a data aberration as it occurs 2-3 sec after the return of visual information. With the exception of the peak, the model vs data comparisons for σ_e are quite good.

The mismatch in $\bar{e}(t)$ for azimuth axis tracking (Fig. 18a) could be explained in terms of a higher order internal model of target motion. This results in a reasonably accurate prediction of target position, at least during the initial phase of blanking. This is plausible in view of a relatively small angular acceleration, $\ddot{\theta}(t) \sim 4.5$ deg/sec^2 at the time of blanking.

One adhoc means to incorporate a higher order internal model within the present OCM structure is to phaseout the observation mechanism in a finite time rather than abruptly. This can be done by effecting the 1-0 transition of the "blanking factor", r(t) exponentially with a non-zero time constant τ_d in Eq. (3.7). An appropriate choice of τ_d was found to be $\tau_d = .005\ \dot{\theta}(\bar{t})/\ddot{\theta}(\bar{t})$, where $\bar{t}$ is the time at which blanking occured.

With the exponential phaseout of the observation mechanism incorporated in the OCM, the model vs data comparisons, although not shown here, were uniformly consistent with the data for both conditions C and D. Although these preliminary results are encouraging, the study of higher order internal models of target motion is an area for future research.

The model vs data elevation axis results for condition C are shown in Fig. 19a-b. The ensemble mean, $\bar{e}(t)$ and standard deviation, $\sigma_e(t)$ exhibit only modest increases. The model replicates these trends quite accurately.

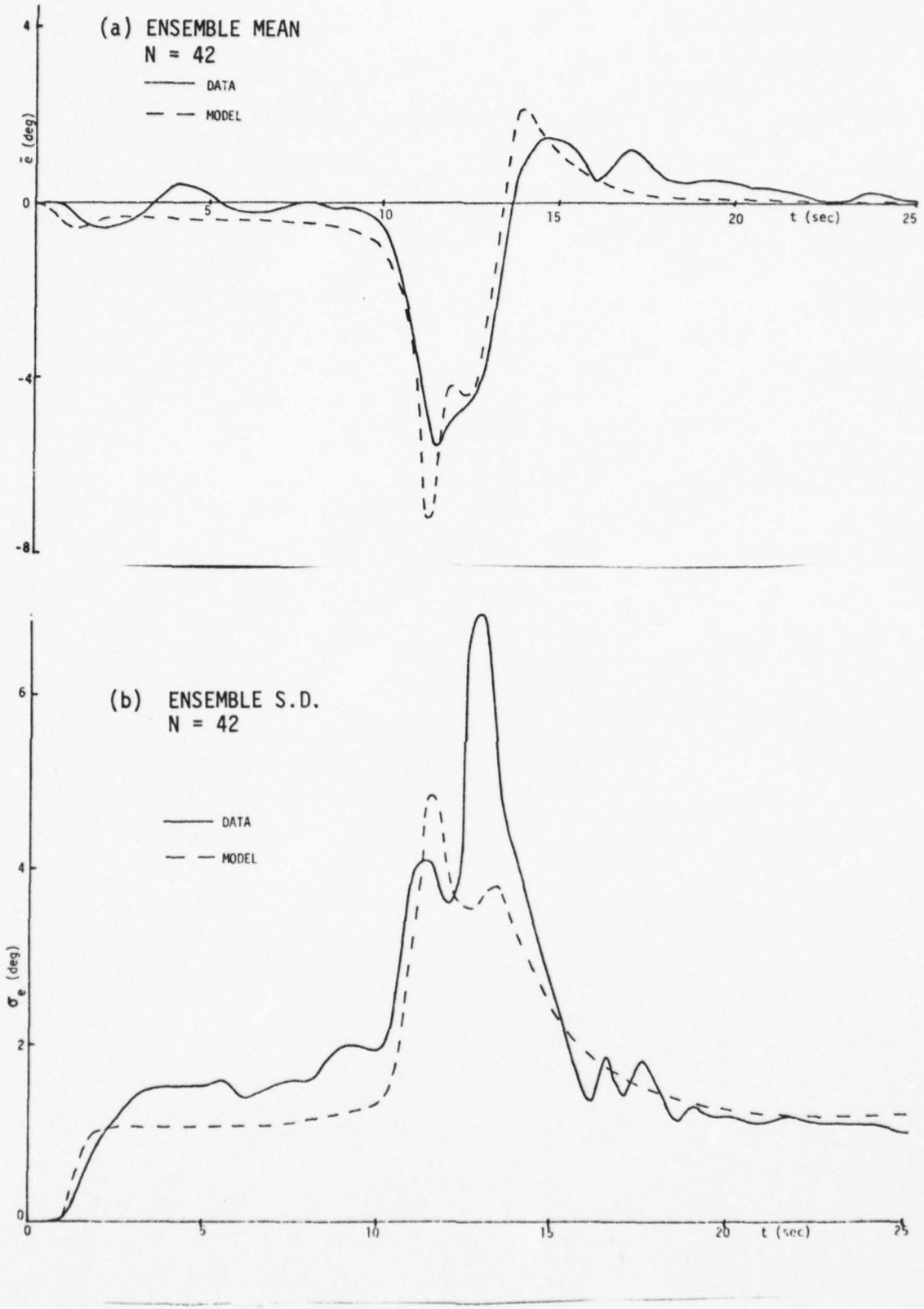

Fig. 18: AZIMUTH AXIS TRACKING, BLANKING AT t=9.79

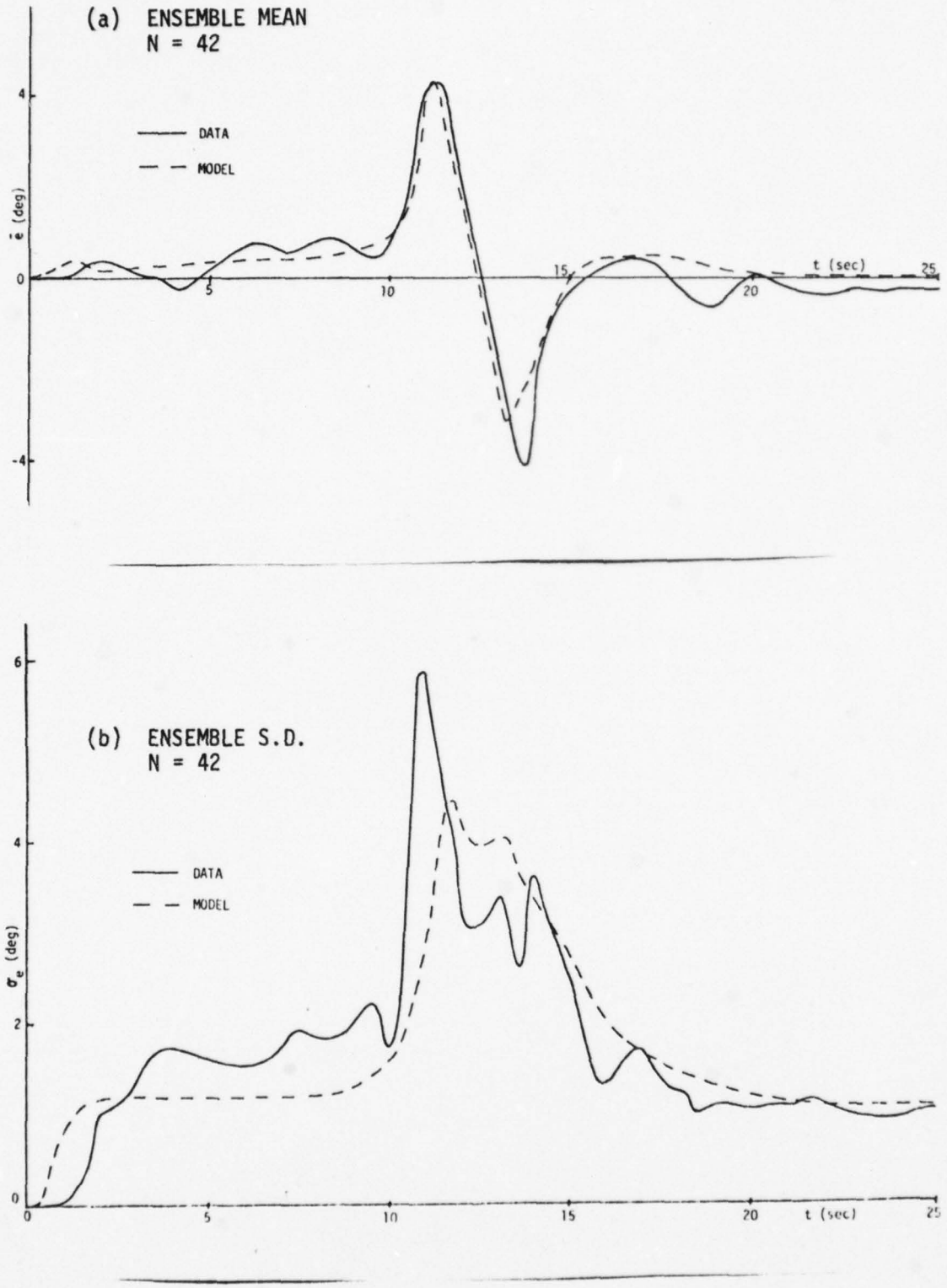

Fig. 19: ELEVATION AXIS TRACKING, BLANKING AT t=9.79

3.5 Discussion and Conclusions

A combined experimental and analytic program has studied simulated target tracking performance as modified by short periods (~1 sec) of target blanking. The blankings occured at pseudo-random times during "straight-and-level" flyby. The information processor associated with the OCM was generalized in a straightforward manner to include the effects of blanking. The model was exercised with a nominal ("off-the-shelf") set of OCM parameters throughout. The model vs data results for the blanking as well as the no blanking cases are very good. The excellent agreement for the no blanking case (Figs. 12-13) are most noteworthy considering the various complex issues such as interaxis attention allocation, visual image cues etc. that have impact on the task. The model vs data blanking results (Fig. 16-19) are extremely encouraging and give credence to the adaptive internal model of Chapter II. Moreover, we have for the first time a quantitative model that can predict the effects of temporary visual obscuration on human tracking performance with reasonable precision.

Extensions of this research include investigation into higher order internal models of target motion, implementation of target obscuration effects into Monte - Carlo simulation of human operator and intermittent blanking of several displays at random times. The last item presents a difficult modeling problem as it involves the interaction between external intermittency (not controlled by human) and human's own internal intermittency or sampling behavior.

IV. TRACKING WITH TRACER INFORMATION

Extensive upgrading of the CYBERLAB facilities, including the acquisition, configuration and interfacing of information processing hardware, and concomitant software development enabled us to explore the problem of ground-to-air tracking with a tracer stream. An experiment was designed, a simulation was developed, and the formal experimental runs were conducted and concluded. The results of these experiments are presented in this chapter.

4.1. Tracer Simulation

A major goal of the current experimental effort was to provide a data base for refining the Optimal Control Model of human response, with emphasis on the human information-processing submodel. In this respect our tracer work is a logical extension of our past research, inasmuch as it addresses important questions of manual tracking system performance. In previous tracking experiments the human controlled a reticle sight to position a cross-hairs on a simulated target. The hypothetical "gun" was assumed to point ahead of the target, the lead angle computed in some manner such that a round fired now would subsequently impact the target. The projectile's ballistic path was never seen by the subject.

Our research focuses on the human's ability to control not the sight, but the projectile path - - i.e. the gun itself. Therefore, in the current effort, the subjects were provided with feedback of hit performance (miss distance) in the form of simulated tracer rounds. From an analytic viewpoint tracers are quite interesting as the error information that they provide is discrete, time-delayed, and non-stationary, as the time-delay is range-dependent. In addition, the human operator must do his own lead-angle prediction, thereby making the tracking task quite difficult. To document tracking performance with tracers, and to provide the necessary data-base for possible future analytic work, we

conducted a set of experiments in which the target (a low-flying aircraft) and the tracers were presented to the subjects as images on a CRT screen. The subjects' control inputs were sampled and stored for off-line analysis of tracking performance.

4.1.1 Experimental Facilities

The CYBERLAB experimental facility consists of a DEC PDP 11/60 computer with 96 KW of MOS memory, cache memory, fast floating-point processor and 7.5 megabyte of on-line disk storage (in addition to a dual-density magnetic tape unit).

The display medium is a DEC VS60 High-Performance Graphics unit, which provides refreshed vector images of extremely high quality on a 21-inch screen. This system features hardware implementation of windowing, which proved especially useful in real-time simulation of the AAA environment (see Sections 4.4-4.5). It provides an 8' x 8' virtual "image definition area", of which any 1' x 1' "window" may be selected by the program for display on the CRT screen.

To sample the subjects' control inputs the Laboratory has twin Air-Force type, force-actuated control grips. These grips, hard-wired into the computer's processor via analog-to-digital converters, are sampled with a resolution of 12 bits (one part in 4096).

4.2. Experimental Set-Up

Each subject in our experiments was seated in front of the 21-inch CRT screen. With the right hand, the subject manipulated a force-actuated (isometric) control stick which generated a rate command to the simulated gun pointing angle. The control stick gain was set to the value which had been judged "most comfortable" during the shakedown runs.

The forcing function $\theta_T(t)$ was the position of a delta-shaped target image during a straight-and-level flyby. The target was assumed to be at a constant altitude of 200 ft., moving from left to right at a constant velocity of 200 mph,

with a cross-over range of 700 ft. At a display-gain value of 1.0 these parameters provided the best trade-off among image size, $\dot{\theta}_T$ and $\ddot{\theta}_T$ (target angular velocity and angular acceleration, respectively).

The subject was assumed to sit between two AA guns, 4 ft. apart. These simulated guns produced two parallel tracer streams on the CRT screen. Tracers were produced at a constant rate of 5 pairs/second throughout the run; the subjects had no control over the simulated firing rate. The muzzle velocity of the tracers was set to 2000 fps and they moved in a ballistic trajectory under the influence of earth gravity. Secondary effects due to air resistance, gyroscopic precession, spin and wind were neglected. The resulting equations of motion of tracer i are, then:

$$x^i(t) = x^i(0) + V_p \cdot \cos\varepsilon^i \cdot \sin\gamma^i \cdot t$$

$$y^i(t) = y^i(0) + V_p \cdot \sin\varepsilon^i \cdot t - 1/2\, gt^2$$

$$z^i(t) = z^i(0) + V_p \cdot \cos\varepsilon^i \cdot \cos\gamma^i \cdot t$$

where (x.y,z) is a cartesian coordinate system centered at the subject with x parallel to the flight-path of the target (positive to the right), y vertical (positive up) and z completing a left-handed triad; V_p is the muzzle speed of the tracers (2000 fps), ε^i and γ^i are the values of the gun's elevation and azimuth angles, respectively, when tracer i was fired, t is tracer i's time of flight and g is the gravitional acceleration (32.2 fps/sec).

Becuase of the inherent limitations of a flat, two-dimensional screen in providing depth cues, tracers were "terminated" (i.e., their images were removed from the screen) when they reached a slant range equal to the target's slant range. Thus, to minimize tracking error[†], or "hit score", the subjects had to point the "gun" in such a way that the end of the tracer-stream coincided with the target's image.

[†]In the present context "tracking error" is defined as the angular distance between the target and tracer stream endpoint as seen by the subject. "Pointing error" refers to the angle between the gun's present position and the perfect position required for a "hit" after a time-of-flight. Thus, present pointing errors give rise to future tracking errors.

The positions (in inertial space) of the simulated target and of each tracer were computed in real time. The corresponding coordinates of their images on the graphics screen were updated at a rate of 20/second. The subjects' control inputs in both azimuth (x) and elevation (y) axes were sampled at the same rate of 20/second and stored in individual disk files for off-line processing. Each run lasted about 25 seconds and produced 512 datum points of each sampled variable.

4.3. Experimental Design

Three experimental conditions were incorporated in the design, as follows:

Condition A: Subject tracks the target with a stream of tracers.

Condition B: Subject sees only the end point of the stream of tracers, displayed as a cross-hairs.

Condition C: Subject sees the full stream of tracers, plus a set of cross-hairs which provides lead-angle information.

Under Condition A, there was no reticle, gun-sight or cross-hairs display. The subjects tracked the target in much the same way as a firefighter would control the stream of water coming out of his hose. Under Condition B the stream of tracers was not visible on the screen; a visible cross denoted the instantaneous end-point of the "invisible" tracers-stream and the subject's task was to place this cross on the target image. Under the third experimental condition the tracers were visible, as under Condition A, but lead-angle information was computed based on the target's present position and velocity (see Section 4.5.). This information was presented to the subject in the form of crosshairs on the screen: When the crosshairs were aligned with the target's image, the tracer round just then leaving the gun would hit the target in a few seconds (time-of-flight). The crosshairs were not stationary on the screen, since the lead angle is a function of the target's present range, relative velocity, etc. The subject thus receives dynamic information as to where to point the "gun".

Each subject received sufficient training in tracking under the above conditions, one Condition at a time. When a subject's performance under an experimental condition reached the desired level he was presented with 15 identical formal runs under that condition before proceeding to the training phase under the next condition. Each subject thus participated in a total of 45 formal runs. The order of presentation of the experimental conditions was counter-balanced among the subjects.

Six subjects, all University of Connecticut students, participated in the formal experiment. All were male, right-handed, with normal vision, and between the ages of 21-25 . Five were Air Force ROTC cadets; two had flying experience, five had sharp-shooting experience.

All of the subjects were highly motivated. To further increase their motivation, however, an imaginary 5' x 9' "bulls-eye" was assumed at the center of the 30' x 15' target aircraft: Only tracers which terminated at this reduced bulls-eye were counted as "hits". At the end of each run the number of hits scored was displayed on the screen (no other performance feedback was provided) and the subject was encouraged to try to do better.

4.4. Image Mapping

In developing the algorithm for mapping the simulated target airplane onto its image on the CRT screen, we took advantage of the hardware-implemented windowing feature of the VS-60 graphics system. This feature provides an 8ft. x 8ft. virtual "image definition area" on which images may be drawn and defined; the program may then specify any sqaure, 1ft. x 1ft., of this virtual area for display on the screen. This displayed 1' x 1' square is known as the "window".

We assumed that the subject was sitting at the center of a sphere of radius ρ, with the 8' x 8' planar image definition area tangent to the sphere. As the subject slewed the simulated gun to an azimuth of γ and elevation angle of ϵ, the planar area rolled around the sphere without slipping in such a way

that the spherical coordinates $(\rho,\gamma,\varepsilon)$ defined the tangency point. This point then served as the center of the window (see Fig. 20). One can now define the fixed coordinate system (x,y,z), with its origin at the center of the sphere, x parallel to the course of the simulated straight-and-level target, y in the vertical direction and z completing a left-handed triad. One can also define the moving system $(\hat{x},\hat{y},\hat{z})$ with its origin at the center of the sphere, $\hat{z}$ passing through the point of tangency, $\hat{x}$ horizontal and $\hat{y}$ completing the left-handed triad. From elementary trigonometry, the coordinates $(\hat{x}_0,\hat{y}_0,\hat{z}_0)$ of any point (x_0,y_0,z_0), i.e. a point on the target, a tracer, etc., are given by

$$\begin{bmatrix} \hat{x}_0 \\ \hat{y}_0 \\ \hat{z}_0 \end{bmatrix} = \begin{bmatrix} 1 & 0 & 0 \\ 0 & \cos\varepsilon & -\sin\varepsilon \\ 0 & \sin\varepsilon & \cos\varepsilon \end{bmatrix} \begin{bmatrix} \cos\gamma & 0 & -\sin\gamma \\ 0 & 1 & 0 \\ \sin\gamma & 0 & \cos\gamma \end{bmatrix} \begin{bmatrix} x_0 \\ y_0 \\ z_0 \end{bmatrix}$$

$$= \begin{bmatrix} \cos\gamma & 0 & -\sin\gamma \\ -\sin\varepsilon\cdot\sin\gamma & \cos\varepsilon & -\sin\varepsilon\cdot\cos\gamma \\ \cos\varepsilon\cdot\sin\gamma & \sin\varepsilon & \cos\varepsilon\cos\gamma \end{bmatrix} \begin{bmatrix} x_0 \\ y_0 \\ z_0 \end{bmatrix} \qquad (4.1)$$

In Fig. 20, M denotes the center of the 8' x 8' image definition area, D is the point of tangency and E is the projection of point (x_0, y_0, z_0) on the image definition area. The horizontal screen coordinate $\underline{ME}$ of point E (horizontal distance from M to E) is then computed as follows:

Via similar triangles,

$$\underline{DE} = \rho \cdot \hat{x} / (\hat{y}^2 + \hat{z}^2)^{1/2} \qquad (4.2a)$$

and since the planar area rolls without slipping,

$$\underline{MD} = \rho\,\gamma \qquad (4.2b)$$

which implies

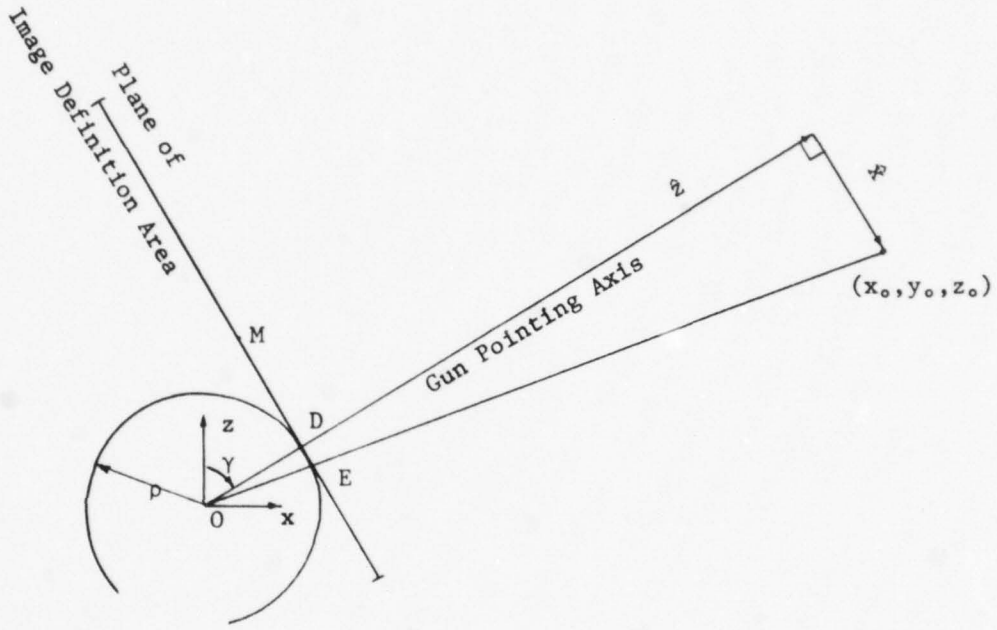

Fig. 20: GEOMETRY OF MAPPING POINT (x_0, y_0, z_0) ONTO THE CRT SCREEN

$$\underline{ME} = \underline{MD} + \underline{DE} = \rho\,[\gamma + \hat{x}/(\hat{y}^2 + \hat{z}^2)^{1/2}] \qquad (4.2)$$

where from (4.1),

$$\hat{x}_0 = x_0 \cos\gamma - z_0 \sin\gamma$$

$$\hat{y}_0 = -x_0 \sin\varepsilon \sin\gamma + y_0 \cos\varepsilon - z_0 \sin\varepsilon \cos\gamma$$

$$\hat{z}_0 = x_0 \cos\varepsilon \sin\gamma + y_0 \sin\varepsilon + z_0 \cos\varepsilon \cos\gamma$$

The computation of the vertical screen coordinate is completely analogous.

4.5. Lead Angles

The lead angles were computed both in azimuth and in elevation assuming that the target would maintain its present attitude and speed, i.e., by a straight-line extrapolation from the target's present position and velocity.

1. Azimuth (see Fig. 21 a):

For an intercept to take place at point I between the tracer and the target, they must reach point I simultaneously, t seconds hence:

$$V'_p \sin\alpha \cdot t = x_T + V'_T \cos\underline{\psi} \cdot t \qquad (4.3a)$$

and

$$V'_p \cos\alpha \cdot t = z_T + V'_T \sin\underline{\psi} \cdot t \qquad (4.3b)$$

where

$V'_p = V_p \cos\varepsilon$, V_p is the tracer's speed, and

ε = the elevation angle of the gun

$V'_T = V_T \cos\theta$, V_T is the target aircraft's speed,

θ = target pitch (flight path) angle

x_T, z_T are the target's present coordinates

$\underline{\psi}$ is the target's heading angle and α, the gun-pointing angle required for an intercept, is as shown in Fig. 21.

Combining (4.3a) and (4.3b) one obtains

$$x_T \cos\alpha - z_T \sin\alpha = \frac{V'_T}{V_p} (x_T \sin\underline{\psi} - z_T \cos\underline{\psi}) \qquad (4.3)$$

and one needs to solve (4.3) for α. To simplify the notation, let

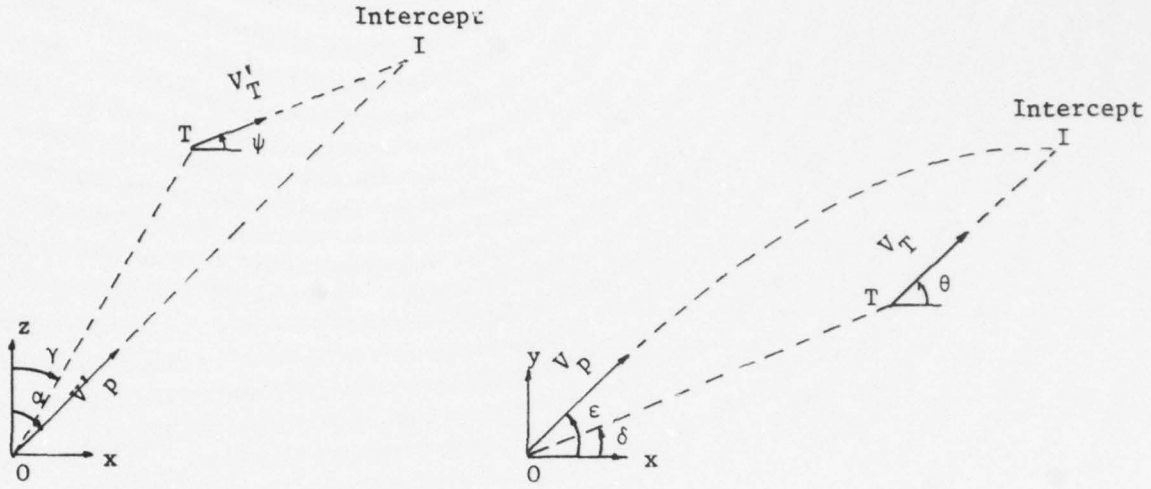

a) top view

b) side view

0 = Observer; origin of (x,y,z) coordinates

γ = present azimuth angle to target

α = future azimuth angle to target

V_T = target speed

V_p = tracers' muzzle velocity

$V'_T = V_T \cos\theta$

$V'_p = V_p \cos\varepsilon$

ε = gun elevation angle

ψ = target heading angle

θ = target pitch (and flight-path) angle

T = target

I = intercept point

Fig. 21: GEOMETRY OF PROJECTILE-TARGET INTERCEPT

$$\zeta \triangleq \frac{x_T}{\frac{V_T'}{V_P'}(x_T \sin\underline{\psi} - z_T \cos\underline{\psi})} \quad , \quad \xi \triangleq \frac{z_T}{\frac{V_T'}{V_P'}(x_T \sin\underline{\psi} - z_T \cos\underline{\psi})}$$

Then (4.3) becomes

$$\zeta \cos\alpha - \xi \sin\alpha = 1 \tag{4.4a}$$

The solution of (4.4a) is straightforward; First, rewrite it as

$$\frac{\zeta}{\sqrt{\zeta^2 + \xi^2}} \cos\alpha - \frac{\xi}{\sqrt{\zeta^2 + \xi^2}} \sin\alpha = \frac{1}{\sqrt{\zeta^2 + \xi^2}} \tag{4.4b}$$

Then let

$$\beta \triangleq \sin^{-1}\left[\frac{\zeta}{\sqrt{\zeta^2 + \xi^2}}\right] = \cos^{-1}\left[\frac{\xi}{\sqrt{\zeta^2 + \xi^2}}\right]$$

and, from (4.4b),

$$\sin\beta \cos\alpha - \cos\beta \sin\alpha = \frac{1}{\sqrt{\zeta^2 + \xi^2}} \tag{4.4c}$$

or,

$$\sin(\beta - \alpha) = \frac{1}{\sqrt{\zeta^2 + \xi^2}} \tag{4.4d}$$

Thus,

$$\alpha = \beta - \sin^{-1}\frac{1}{\sqrt{\zeta^2 + \xi^2}} \tag{4.4}$$

substituting in (4.4) for β, ζ^2 and ξ^2 one gets

$$\alpha = \sin^{-1}\frac{x_T}{\sqrt{x_T^2 + z_T^2}} - \sin^{-1}\frac{\frac{V_T'}{V_P'}(x_T \sin\underline{\psi} - z_T \cos\underline{\psi})}{\sqrt{x_T^2 + z_T^2}} \tag{4.5}$$

but, from simple geometry, $\sin^{-1}\frac{x_T}{\sqrt{x_T^2 + z_T^2}} = \gamma$; $\frac{z_T}{\sqrt{x_T^2 + z_T^2}} = \cos\gamma$,

where γ is the present azimuth angle to the target. Substituting these values in (4.5) results in

$$\alpha = \gamma - \sin^{-1} \frac{V_T'}{V_p'} [\sin\gamma \sin\underline{\psi} - \cos\gamma \cos\underline{\psi}] \tag{4.6a}$$

or

$$\alpha = \gamma - \sin^{-1} \frac{V_T'}{V_p'} [-\cos(\underline{\psi} + \gamma)] \tag{4.6b}$$

and, finally

$$\alpha = \gamma + \sin^{-1} \left[\frac{V_T \cos\theta}{V_p \cos\varepsilon} \cos(\underline{\psi} + \gamma) \right] \tag{4.6}$$

Note that ε in (4.6), the gun elevation angle required for an intercept, is not yet known.

2. Elevation (see Fig. 21 b):

$$V_p \sin\varepsilon \cdot t - 1/2\, gt^2 = y_T + V_T \sin\theta \cdot t \tag{4.7a}$$

where ε is the gun elevation angle required for an intercept at point I, g is the acceleration of gravity and y_T is the target's present vertical coordinate. Equation (4.7a) can be solved for ε:

$$\varepsilon = \sin^{-1} \left[\frac{y_T + V_T \sin\theta . t + 1/2\, gt^2}{V_p t} \right] \tag{4.7}$$

and t in (4.7) can be found either from (4.3b) or from (4.3a). An iterative procedure is than suggested as follows:

1. Assume $\varepsilon_{n-1} = \delta$ (see Fig. 21b),

2. $\alpha_n = \gamma + \sin^{-1} \left[\frac{V_T \cos\theta}{V_p \cos\varepsilon} \cos(\underline{\psi} + \gamma) \right]$ from Eq. (4.6),

3. $t_n = \frac{z_T}{V_p \cos\varepsilon \cos\alpha - V_T \cos\theta \sin\underline{\psi}}$ from Eq. (4.3b),

4. $\varepsilon_n = \sin^{-1} \left[\frac{y_T + V_T \sin\theta \cdot t - 1/2gt^2}{V_p t} \right]$ from Eq. (4.7),

5. If $|\varepsilon_n - \varepsilon_{n-1}| > r$ then go back to 2

With r, the convergence criterion, set to 10^{-5} radians the iterative procedure converges in 3-5 iterations. This computation is done on-line for condition C, and the angular position of the cross-hairs is displaced (α, ε) from where the gun is now pointing. Thus, if the cross-hairs are centered on the target the "gun" will, per-force, be leading by (α, ε) as required.

4.6. Data

Five variables were sampled and stored during each formal run: the (x,y,z) coordinates of each tracer as it reached a slant range equal to the target's, and the control stick inputs in azimuth and elevation. At a sampling rate of 20/second, each 25.575-sec. run resulted in 512 datum points for each of these five variables. In addition, header information was recorded for each run, consisting of date and time of run, subject identification code, experimental condition data, etc.

Note that the variable of greatest interest, namely, the tracking error or miss distance, was not recorded. This variable could be reconstructed from the recorded data off-line and thus, in an attempt to minimize disk storage requirements, was not stored explicitly.

Tracking error (or, more accurately, "miss angle") could be computed from the coordinates of the "last" tracer (that is, the tracer which had just reached the target's slant range): as the target's trajectory was deterministic its coordinates could be computed and compared with the coordinates of the corresponding "last" tracer, to yield angular error. This approach, however, was abandoned for three main reasons:

1. There is no guarantee that a tracer would reach a slant range equal to the target's every sampling interval (1/20 sec.).
2. At a muzzle velocity of 2000 fps a tracer travels about 100 ft. during each sampling interval; the target travels approximately 15 ft. in the same time.

Thus a tracer's coordinates are accurate to within ± 50 ft., and the target's- to within ± 7.5 ft., yielding inaccuracies and noise in the resulting miss angle. Although these inaccuracies may be minimized by some curve-fitting interpolation techniques, the procedure is complicated and cumbersome.

3. This technique yields a value for the miss angle, e(t), at time t when a tracer reaches the target's slant range. As far as the subject's performance is concerned, however, the error is attributable to the time $(t-\tau)$ when that tracer left the gun, τ being the tracer's time of flight. The time-shift τ is not constant, as it is a function of the target's slant range. As a consequence, translating the error sequence e(t) in time to generate the sequence $e(t-\tau)$ may prove to be a complicated and cumbersome proposition.

Instead, a different algorithm was employed to compute the gun-pointing error: Based on the target's trajectory (which was deterministic) a sequence of perfect lead-angles was generated off-line (see Section 4.5), i.e., angles at which the gun should be pointing in order for the tracer just-then being fired to hit the target. These values were subtracted from the corresponding (recorded) actual control inputs to yield the desired pointing-error sequence.

When the target's motion is completely known (as it was in our experiments), and when the computation of the lead-angles sequence is based on that known target motion (as it was in this case), then it can be shown that the gun-pointing -error sequence is equivalent to the sequence $e(t-\tau)$ of item (3) above. In other words, a gun-pointing-error e_i at the time a tracer leaves the gun gives rise to an equal miss-angle τ seconds later, when that tracer reaches the target's slant range.

As a check, the two methods (that of "miss angles" and that of "pointing errors") were compared. They proved to be equivalent, apart from the time-varying time-shift τ. However, the lead-angle, gun-pointing-error method produced noticeably smoother results. All the results shown in this report in graph form are gun-pointing-errors, derived by the lead-angle method.

4.7. Results and Discussion

As a first step in analyzing the results the data were aggregated, i.e., point-by-point ensemble means and mean-squares were computed. We utilized a sequential approach to the computation, by which the mean m^j_{k+1} of the j-th point ($0<j\leq 512$) of k+1 runs was computed from m^j_k by

$$m^j_{k+1} = (m^j_k \cdot k + z^j_{k+1}) / (k+1) \tag{4.8}$$

where z^j_{k+1} is the value of the j-th point in the (k+1)-th run, and $m^i_1 = z^i_1$, $i = 1, 2 \ldots 512$.

The mean-square q^j_{k+1} was computed similarly from q^j_k by

$$q^j_{k+1} = (q^j_k \cdot k + (z^j_{k+1})^2) / (k+1) \tag{4.9}$$

and the unbiased estimate of the variance, v^j_k, was then found from

$$v^j_k = (q^j_k - (m^j_k)^2) \cdot k/(k-1) \tag{4.10}$$

Outliers were identified and removed prior to the averaging process: As the CRT screen subtended a visual angle of approximately $\pm 13^\circ$, tracking errors of magnitudes larger than 13° indicated loss of the target's image. We set the cutt-off point, somewhat arbitrarily, at 3 seconds: Any run containing a tracking error (in either axis) in excess of 13° for more than 3 seconds was labeled an outlyer and removed from the statistics. A total of five runs were thus removed (1 from Condition "A" and 2 each from Conditions "B" and "C"). The surviving runs are grouped at the end of this section. As expected, tracking performance was best under Condition "C" (presence of lead-angle information). Unexpected, however, were some characteristics of the data, such as:

1. The tracking performance with only end-point information is much worse than the performance when the full tracer-stream is visible: Peak azimuth errors under Condition B are three times larger than the corresponding error under Condition A. This fact came to us as an unexpected surprise, as the tracer-stream had not been thought to contain useful

information apart from its end point. Obviously, it does, and this may be a useful area for future investigation.

2. In departure from our practice in previous years, the runs of this experiment commenced with a non-zero initial error, both in azimuth and in elevation, of about 1°. Invariably, this initial error effected an overshoot of about 2° under conditions A and B (there was no overshoot with lead-angle information), indicating perhaps some lack of tightness in the control loop even in this region of so-called "good tracking".

3. The error variance exhibits an interesting behavior: Under Condition C (lead-angle information) it is low throughout, except for some increase in the cross-over region. Under conditions "A" and (especially) "B", however, the variance shows a tendency to increase with time (Figs. 24-5). This tendency is especially evident in individual subjects' statistics (such as Fig. 28), where this trend is not masked by inter-subject variability.

The phenomenon of an increased variance without a correlated change in the mean is typical of unstable oscillatory behavior, such as oscillations with increasing amplitude. Keeping in mind the nature of the task, namely tracking a moving target with a stream that is, in effect, a long and flexible "hose", one can suspect such instability as the"hose length" increases. It may be rooted in the increasing time-delay, which effects a limit-cycle behavior equivalent to pilot-induced oscillations (PIO). It is less clear why this behavior is more promounced under Condition "B", with only end-point information, as compared to Condition A (full stream). The question of the particular mechanism of the damping, evident when the full tracer stream is visible, as well as the causal relationship between the magnitude of the time-delay and the instability, remain yet to be explored.

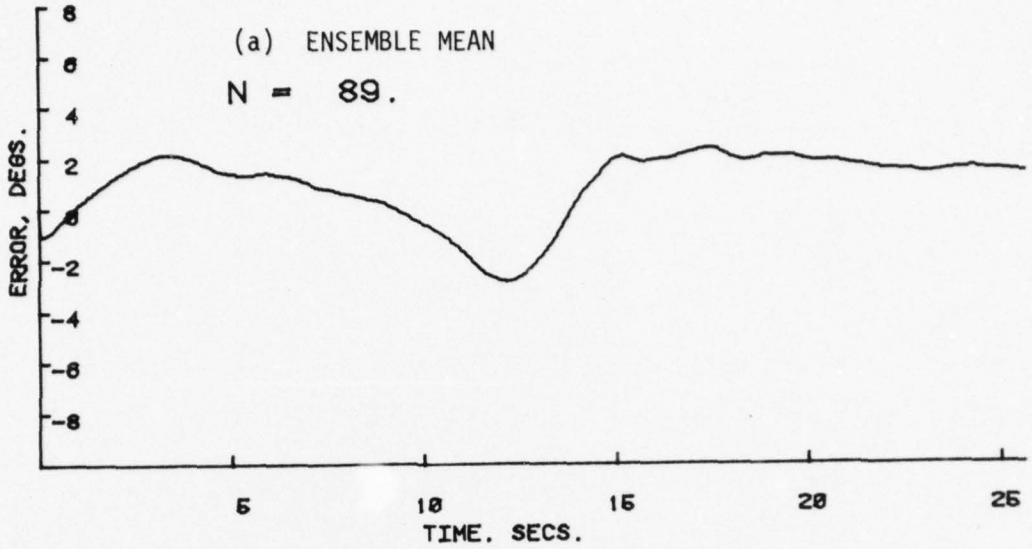

Fig. 22: AZIMUTH AXIS POINTING ERROR, FULL TRACER-STREAM

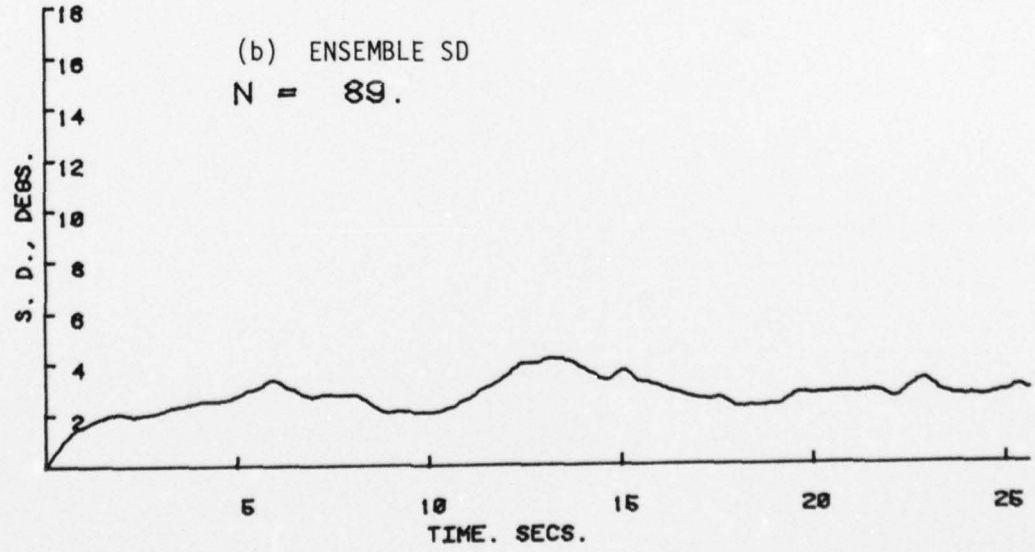

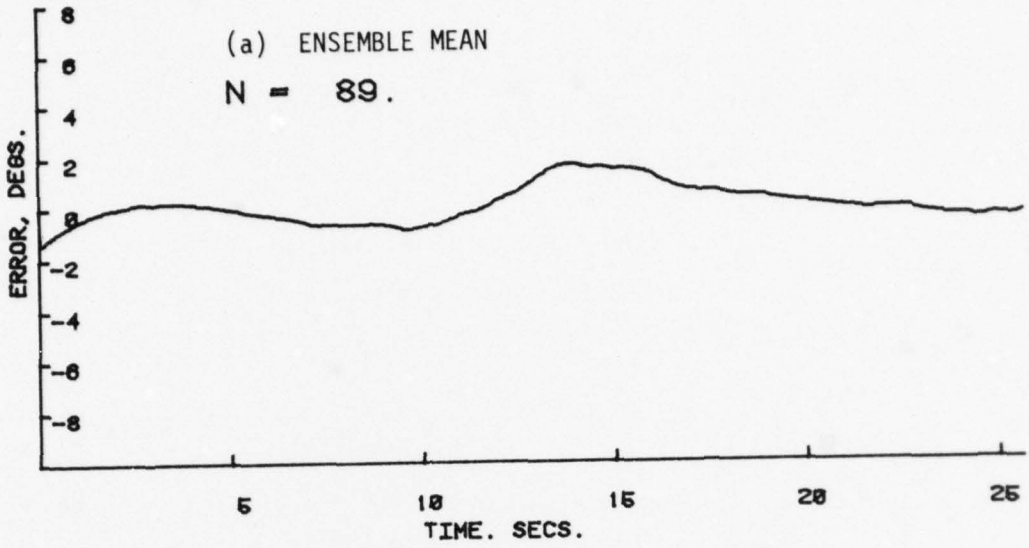

Fig. 23: ELEVATION AXIS POINTING ERROR, FULL TRACER-STREAM

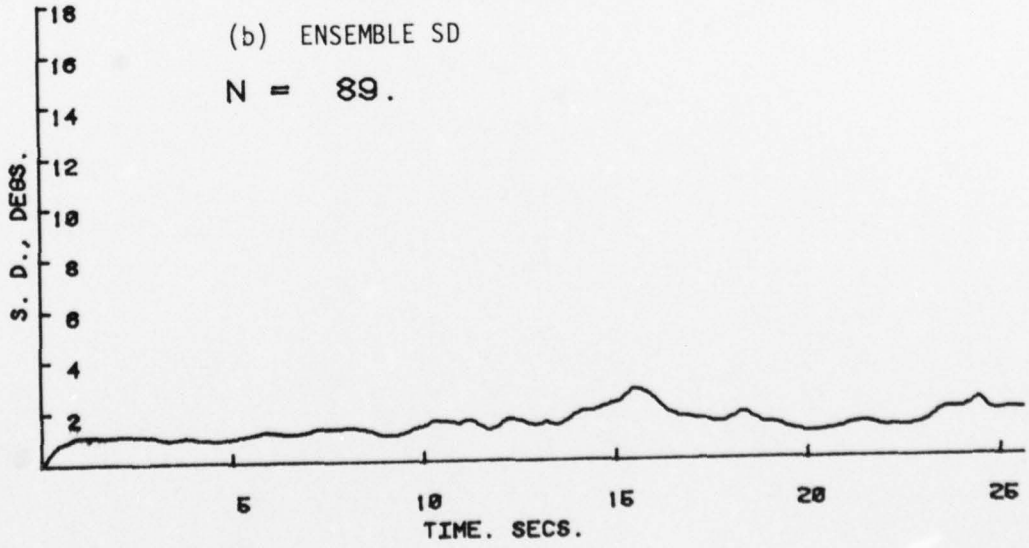

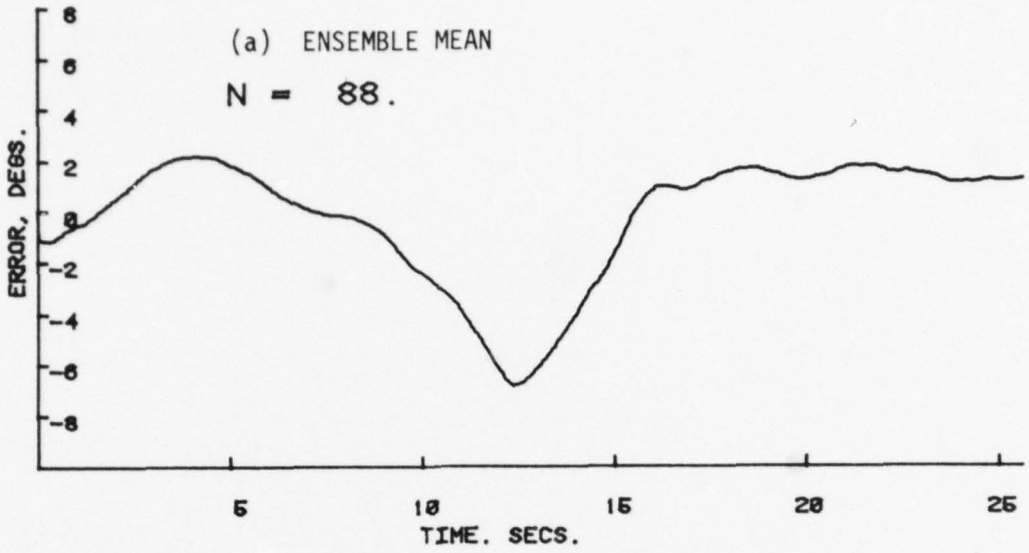

Fig. 24: AZIMUTH AXIS POINTING ERROR, TRACER-STREAM END-POINT ONLY

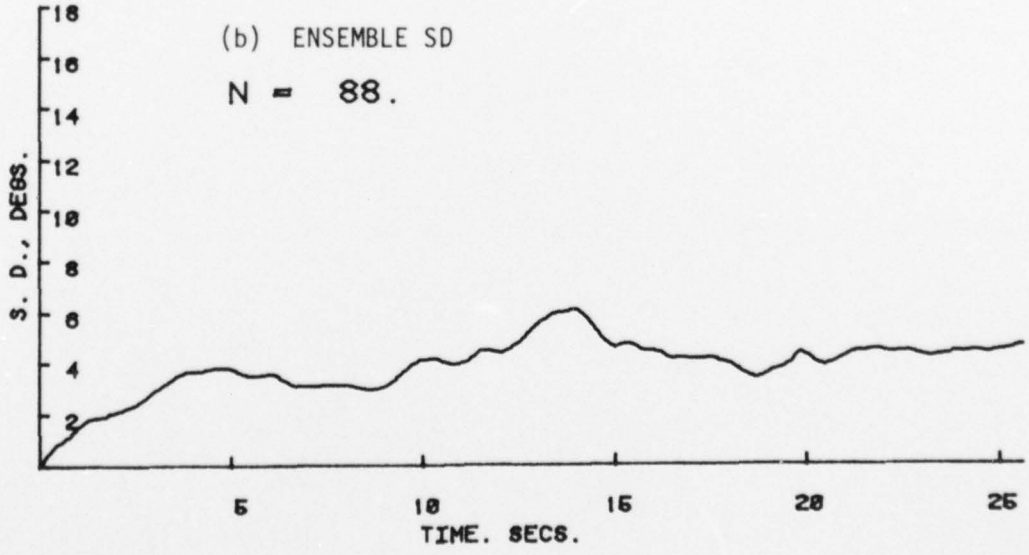

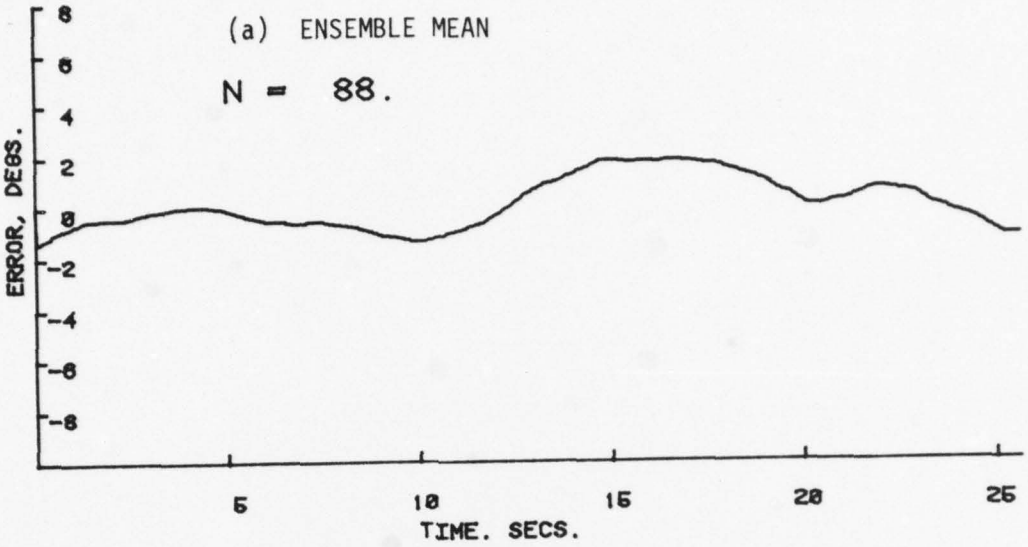

Fig. 25: ELEVATION AXIS POINTING ERROR, TRACER-STREAM END-POINT ONLY

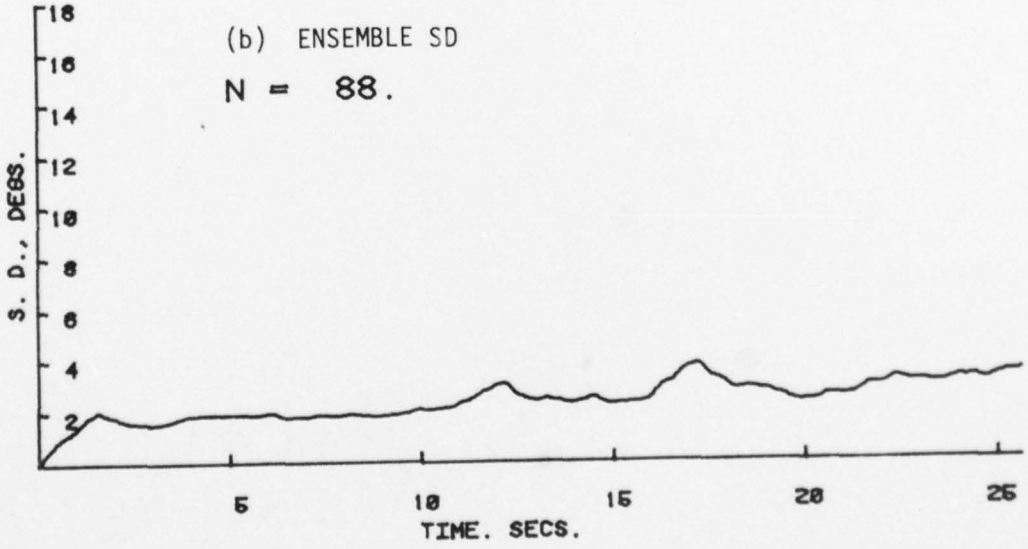

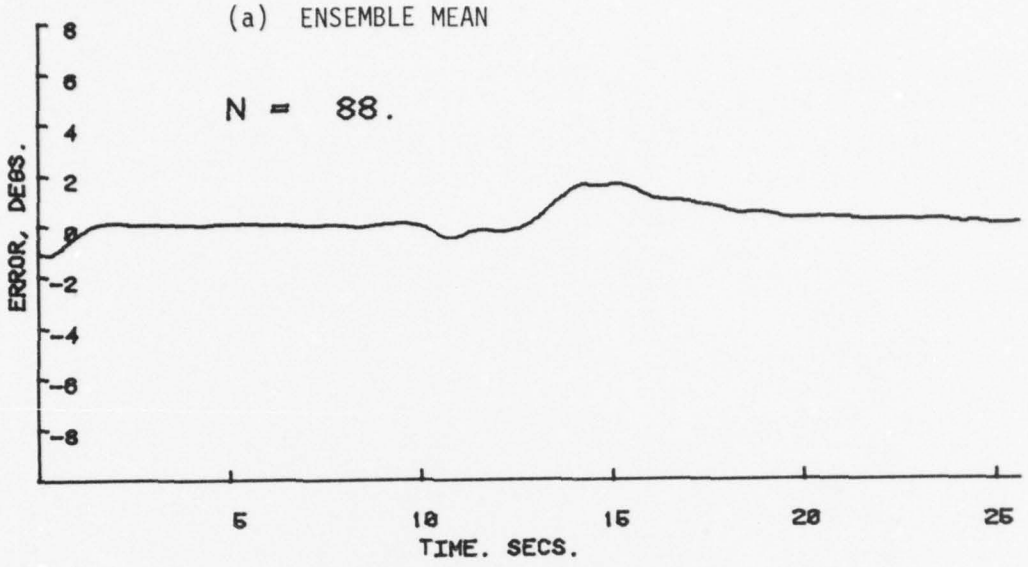

Fig. 26: AZIMUTH AXIS POINTING ERROR, LEAD-ANGLE INFORMATION

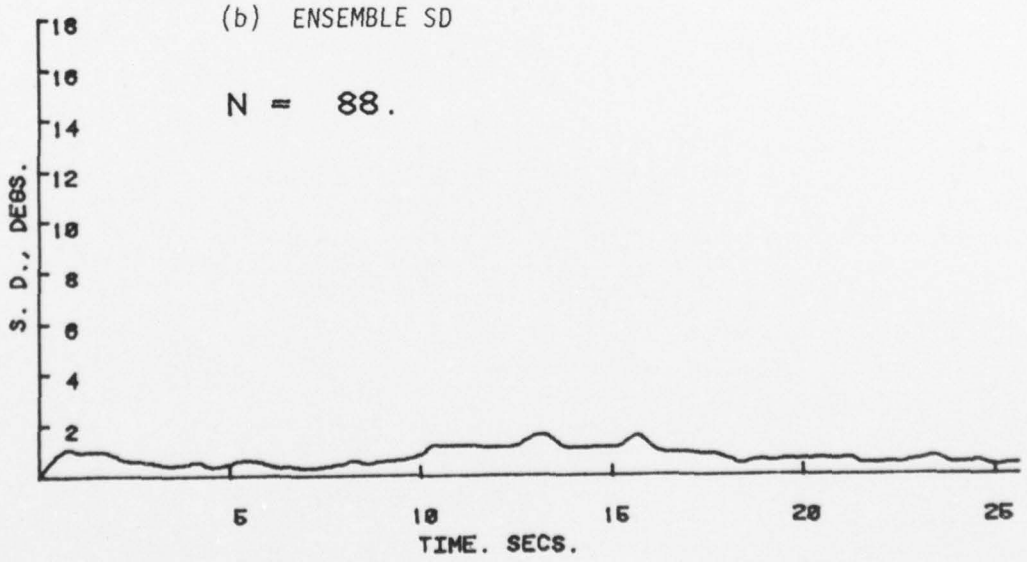

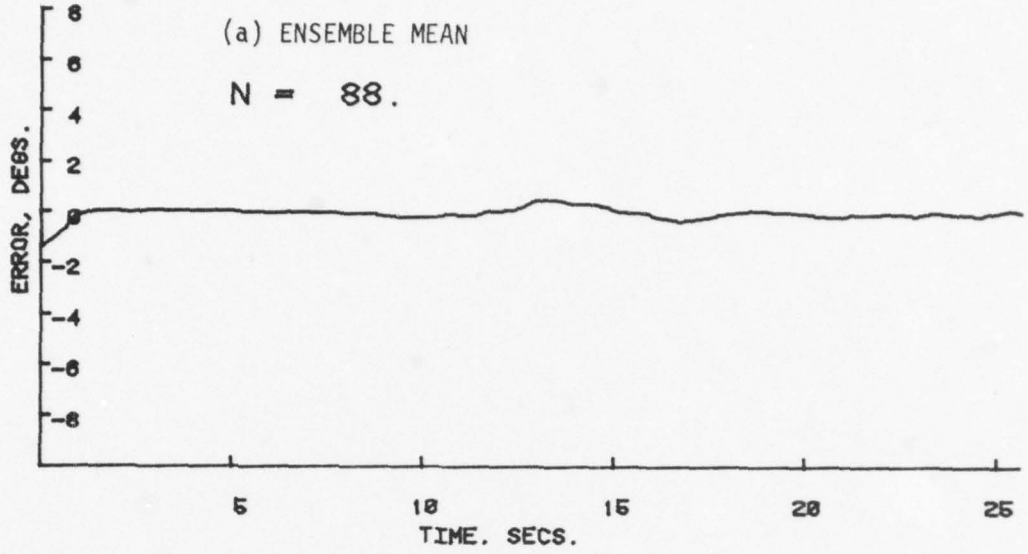

Fig. 27: ELEVATION AXIS POINTING ERROR, LEAD-ANGLE INFORMATION

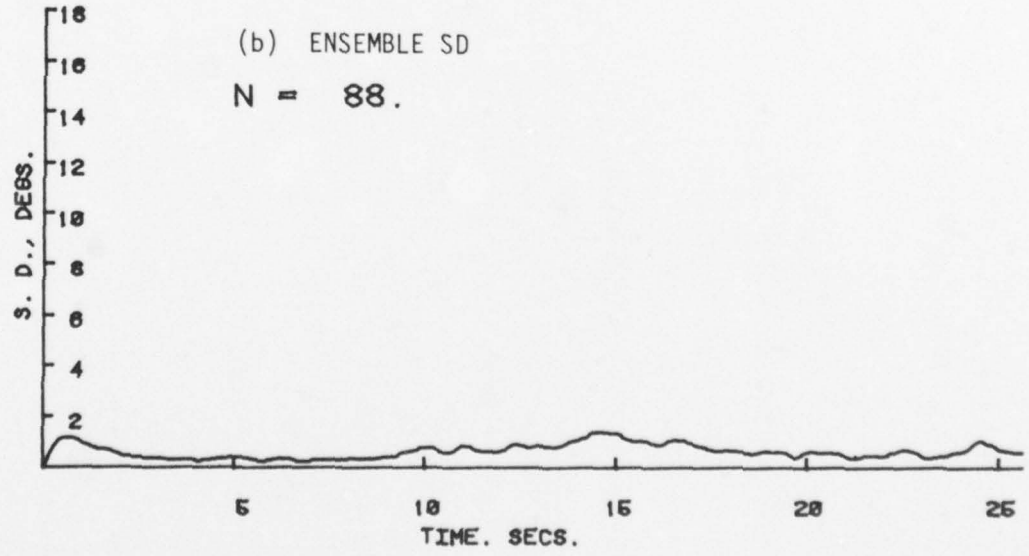

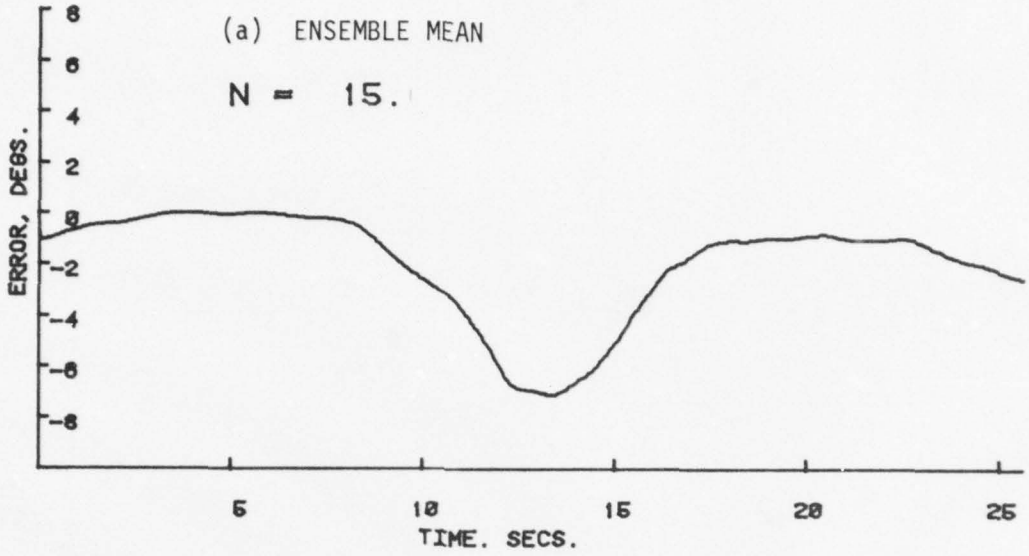

Fig. 28: SUBJECT DG, AZIMUTH AXIS POINTING ERROR, TRACER-STREAM END-POINT ONLY

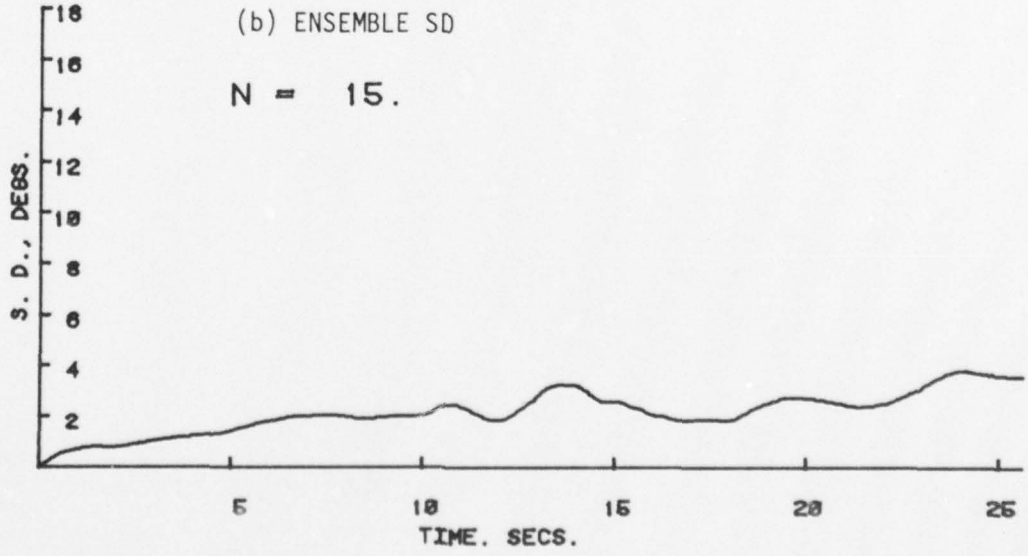

V. CONCLUSIONS AND RECOMMENDATIONS

The results of a joint experimental and analytic program were assimilated into a precision Optimal Control Model for predicting manual performance in a simulated AAA tracking system. The model that has emerged from this study represents the state-of-the-art with regard to human performance modeling in such man-machine systems. It can treat arbitrary target flybys, single-vs-dual axis tracking, visual image cues, and even the effects of temporary visual obscuration. It can be used with confidence to predict the operator's control performance in manned tracking tasks, under assumptions of different tracking system/display configurations, etc.

With respect to one aspect of the present study, our model predicts that stylized image cues will significantly improve performance in a single-operator system, but will have little effect in a two-operator system. It would seem appropriate, therefore, to consider further analytic/experimental efforts that deal with display augmentation for performance improvement. These added cues could be target-related ($\dot{\theta}_T$, $\ddot{\theta}_T$, etc.), or error-related ($\dot{e}$, miss-distance, etc.). Typical of added cues are explicit display of target velocity vector, moving background scene or checker-board grid, target position extrapolator, etc.

A major factor in the success of the present effort was the description of the operator's "internal model" of the target motion. Target blanking experiments were devised that would accentuate the role of this internal model in the manual tracking response. The mathematical construct of the model involved the use of adaptive techniques for on-line estimation of signal bandwidth.

The concept of an "internal model" in manual control and decision-making contexts has long been recognized by engineering and experimental psychologists. However, methods for quantifying this construct in a way that would be applicable

to analytic modeling are rare. Jagacinski and Miller [22] provided what is perhaps the first attempt to quantify a human operator's internal model of a dynamic system within an optimal control-theoretic context. Their results showed striking differences between internal and actual models -- differences that exhibited orderly changes with practice. Their results, plus those of the present effort show that it is possible to infer an operator's internal model within a normative optimal control context. If certain assumptions are made relative to what manual control should accomplish (e.g. as in the OCM), then consistent differences between normative and actual responses can be attributed to the internal model construct.

One drawback to the Optimal Control Model is its complexity -- a direct and necessary result of its completeness. However, this complexity stands as a possible impediment to its use by a wider community of engineers and analysts, especially if routine, repetitive use of the model is contemplated for a specific configuration. In such cases, the OCM should be simplified to the maximum extent possible while maintaining its performance-predictive quality. This obviously limits the scope of the model, but the context-oriented application is now simpler numerically. Initial efforts to build a simplified tracking error model, using reduced-order observer theory, have shown promise [23]. Further work in this area is recommended in order to strengthen the interface between the "model-builders" and the "model-users".

Our experimental investigations of human operator tracking using a tracer stream were directed towards overall system performance, using as a metric actual hit score. Controlling the tracers was found to be a very difficult task that could certainly benefit from the use of system/display augmentation. Our experiments showed human operator performance improves substantially when the full trac stream is visible (as opposed to just the endpoint). This suggests further analys

of the information content, visual cues, and/or stabilizing features contained in a full (or partial) stream.

The explicit display of lead-angle information (using a disturbed reticle approach) was found to give significant improvement in hit score. This is not too surprising considering the fact that a straight-and-level flyby was used, so that perfect lead-angle computing was possible. Nevertheless, this work indicates that the relatively poor lead angle predicting capability of a human can be augmented. When combined with the good tracking ability of a trained operator, a hybrid configuration can offer significant overall performance. Further work in this area is needed to describe analytically the closed-loop dynamics of the human/tracer tracking loop. Experimental efforts are needed to provide a more extensive data base, and to explore different configurations (e.g., dual operator with lead angle adjustment, use of computer-estimated accelerations for lead angle or future position indicators, etc.). The object of this research is to find the optimum balance between man and computer to maximize overall system effectiveness. A prerequisite to accomplish this goal is a research model that describes human information processing and control behavior in tracking tasks -- such a model is now available through this effort.

REFERENCES

1. Tustin, A., "The Nature of the Operator's Response in Manual Control and its Implications for Controller Design", Journal of IEE, Vol. 94, 1947.

2. Kleinman, D.L., Baron, S., and Levison, W.H., "A Control Theoretic Approach to Manned-Vehicle Systems Analysis", IEEE Trans. Autom. Control, Vol. AC-16, No. 6, 1971.

3. Kleinman, D.L., and Perkins, T.R., "Modeling Human Performance in a Time-Varying Anti-Aircraft Tracking Loop", IEEE Trans. AC, Vol. AC 19, No. 4, Aug. 1974.

4. Phatak, A.V., and Kessler, K.M., "Formulation and Validation of a PID Structure Modified Optimal Control Model for the Human Gunner in an AAA Tracking Task", Proc. 1976 Decision and Control Conference, Clearwater, Fla.

5. Kleinman, D.L. and Glass, B., "Modeling AAA Tracking Data Using the Optimal Control Model", 13th Annual Conference on Manual Control, M.I.T., June 1977.

6. Kleinman, D.L., and Ephrath, A.R., "Effects of Target Motion and Image on AAA Tracking ", Proc. 1977 IEEE Conference on Decision and Control, New Orleans.

7. Kleinman, D.L., Ephrath, A.R., Krishna Rao, P., "Effects of Target Motion and Image on AAA Tracking", Univ. of Conn., Dept. of EECS, TR 77-7, Nov. 1977.

8. Kleinman, D.L., "Covariance Propagation Equations for the Optimal Control Model:, Univ. of Conn., Dept. of EECS, TR-77-6, Sept. 1977.

9. Kleinman, D.L., "Solving the Optimal Attention Allocation Problem in Manual Control, IEEE Trans. AC, Vol. AC-21, No. 6, Dec. 1976.

10. Kleinman, D.L., "Monte-Carlo Simulation of Human Operator Response", Univ. of Conn., Dept. of EECS, Tech. Report TR-77-1, Feb. 1977.

11. Lancraft, R.E. and Kleinman, D.L., "A Comparison of Motor Submodels in the Optimal Control Model", Proc. 14th Annual Conference on Manual Control, USC, April 1978.

12. Lancraft, R.E., "A Comparative Study of Neuromotor Models in Manual Control", MS Thesis, Dept. of EECS, University of Connecticut, Jan 1979.

13. Kleinman, D.L. and Baron S., "Manned Vehicle Systems Analysis by Means of Modern Control Theory", NASA CR-1753, June 1971.

14. Levison, W.H. and Junker, A.M., "A Model for the Pilot's Use of Motion Cues in Roll-Axis Tracking Tasks", AMRL-TR-77-40, June 1977.

15. Lee, G.K., Wittenmark, B. and Kleinman, D.L., "Identification of Parameters in the Optimal Control Model", Proc. 14th Annaul Conference on Manual Control, USC, April 1978.

16. Lancraft, R.E. and Kleinman, D.L., "On the Identification of Parameters in the Optimal Control Model", Proc. 15th Annual Conference on Manual Control, Dayton Ohio, March 1979.

17. Gottsdanker, R.M., "The Accuracy of Prediction Motion", J. Exp. Psych., Vol. 43, 1952.

18. Hammerton, M. and Tickner, A.H., "The Effect of Temporary Obscuration of the Target on a Pursuit Tracking Task", Ergonomics, Vol. 13, No. 6, 1970.

19. Pew, R.W., "Performance of Human Operators in a Three-State Relay Control System with Velocity-Augmented Displays", IEEE Trans. Human Factors, Vol. 7, No. 2, 1966.

20. Eaton, J.H., "Discrete-time Interrupted Stochastic Control Processes", J. of M. Anal. and Appl., Vol. 5, 1962.

21. Baron, S. and Berliner, J., "Manmod 1975: Human Internal Models and Scene-Perception Models", Technical Report RD-CR-76-3, U.S. Army MICOM, Redstone Arsenal.

22. Jagacinski, R.J. and Miller, R.A., "Describing the Human Operator's Internal Model of a Dynamic System", Human Factors, Vol. 20, No. 4, 1978.

23. Kou, R.S. et al., "Development of an AAA Gunner Model Based on Reduced-Order Observer Theory", Proc. 1978 IEEE Conference on Decision and Control, San Diego, Calif.